THEORETICAL AND EXPERIMENTAL VIBRATIONAL AND NMR STUDIES OF α AND β-RDX

By

Ricardo Infante Castillo

A thesis submitted in partial fulfillment of the requirements for the degree of

DOCTOR OF PHILOSOPHY
In
Applied Chemistry
(Materials)

UNIVERSITY OF PUERTO RICO
MAYAGÜEZ CAMPUS
2008

Approved by:

_____	_____
Miguel E. Castro Rosario, Ph.D. Member, Graduate Committee	Date
_____	_____
Nairmen Mina Camilde, Ph.D. Member, Graduate Committee	Date
_____	_____
Luis A. Rivera Montalvo, Ph.D. Member, Graduate Committee	Date
_____	_____
Julio G. Briano Peralta, Ph.D. Member, Graduate Committee	Date
_____	_____
Samuel P. Hernández Rivera, Ph.D. President, Graduate Committee	Date
_____	_____
Narinder K. Mehta Chopra, Ph.D. Representative of Graduate Studies	Date
_____	_____
Francis Patrón Geoghegan, Ph.D. Chairperson of the Department of Chemistry	Date

ABSTRACT

Cyclic nitramine hexahydro-1,3,5-trinitro-*s*-triazine (RDX), is an important energetic ingredient for propellants and explosives. To understand RDX explosive nature, the molecular structure needs to be examined in detail. Solid state RDX exist as three polymorphs: α, β and γ. The α-form is the stable polymorph at room temperature with C_s symmetry, β-polymorph has a molecular symmetry of C_{3v} and γ- polymorph may assume one of three orthorhombic structures: D_{2h}, C_{2v} or D_2. Solid state Infrared and Raman spectra of α-RDX and ^{13}C and ^{15}N (ring) enriched isotopomers were recorded and fundamental frequencies were assigned using isotopic frequency shifts. Changes in vibrational signals associated with isotopic substitutions provide nearly unambiguous assignments of vibrational spectra of α-RDX, particularly where exact nature of vibrational modes had been either vague or contradictory. Assignments of the vibrational modes for α and β-RDX were made through comparisons between experimental and density functional calculations results. Calculated frequencies represent vibrational signatures for gas phase molecules. Hence, experimentally observed spectra for solid α and β-RDX may differ somewhat from calculated spectra for RDX AAE and AAA conformers. In the DFT calculation, B3LYP function tends to overestimate the spectral location of vibrational bands compared to experimentally observed values. The slight disagreement between theory and experiment could be a consequence of anharmonicity and of the

general tendency of quantum chemical methods to overestimate force constants at the equilibrium geometry.

The elusive $\alpha \rightarrow \beta$ solid-solid RDX phase transition has been documented in real time mode using Raman spectroscopy. The thermal conversion of $\alpha \rightarrow \beta$ at atmospheric pressure occurred at 204°C. The vibrational pattern of solid β-RDX shows that several vibration signals present in α-RDX phase coalesce into single, doubly degenerate vibrations, possibly because of higher molecular symmetry.

Calculated nuclear magnetic resonance (NMR) chemical shifts (^{13}C and ^{15}N) are reported for RDX conformers and others cyclic and acyclic nitramines. Data were compared with experimental solid and solution data, focusing on agreement of spectral patterns and trends. In order to establish a convenient and consistent protocol to be employed for confirming experimental ^{13}C and ^{15}N NMR spectra of nitramine compounds, different combinations of models and basis set were considered.

RESUMEN

La nitramina cíclica hexahidro-1,3,5-trinitro-s-triazina (RDX) es un ingrediente energético importante en explosivos e impulsores. Para entender su naturaleza explosiva la estructura molecular debe examinarse detalladamente. RDX presenta tres polimorfos sólidos: α, β y γ. La forma α es el polimorfo estable a temperatura ambiente con simetría C_s; el polimorfo β tiene simetría C_{3v}; el polimorfo γ puede asumir estructura ortorrómbicas: D_{2h}, C_{2v} o D_2. Cambios en modos vibracionales asociados con sustituciones isotópicas permiten asignar espectros infrarrojo y Raman de α-RDX casi sin ambigüedad, especialmente donde la naturaleza exacta de los modos vibracionales ha sido confusa o contradictoria. Se midieron espectros Infrarrojo y Raman en estado sólido de α-RDX e isotopómeros enriquecidos ^{13}C y ^{15}N (anillo) y se asignaron frecuencias fundamentales utilizando desplazamientos isotópicos. Las asignaciones de los modos vibracionales para α and β-RDX se realizaron por comparaciones de resultados experimentales y cálculos de densidad funcional. Las frecuencias calculadas representan señales vibracionales de moléculas en fase gaseosa. Espectros observados experimentalmente de sólidos α-RDX y β-RDX pueden diferir parcialmente de espectros calculados para confórmeros AAE y AAA. En cálculos de teoría de densidad funcional (DFT), la función B3LYP tiende a sobreestimar la localización de vibraciones fundamentales comparadas con mediciones experimentales. Desacuerdos entre teoría y experimentos pueden ser consecuencia de anharmonicidad y la tendencia general de métodos de

química cuántica de sobreestimar constantes de fuerza en geometrías de equilibrio.

La transición de fase sólido-sólido α-RDX$\rightarrow\beta$-RDX se observó y documentó en tiempo real utilizando espectroscopia Raman. La conversión térmica ocurre a 204°C a presión atmosférica. El patrón vibracional de β-RDX sólido muestra que algunos modos presentes en la fase α-RDX, son vibraciones doblemente degeneradas, que aparecen como sencillas debido a aumento en simetría molecular.

Se informaron cálculos desplazamientos químicos de resonancia magnética nuclear (RMN) para ^{13}C y ^{15}N en confórmeros de RDX y otras nitraminas cíclicas. Los datos comparados con valores experimentales en sólido y solución se analizaron con base a patrones y tendencias espectrales. Con el fin de establecer un protocolo consistente y conveniente para emplearse al confirmar espectros experimentales RMN de ^{13}C y ^{15}N de nitraminas, se utilizaron diferentes combinaciones de modelos y bases.

In memory to my grandfather Nabor Infante Puerto.
To my kids Manuel Alejandro and Ricardo Andres, for being my inspiration.
To my wife Brenda, for her patience and support.
To my parents and sisters for their unconditional support.

ACKNOWLEDGEMENTS

During the development of my doctoral studies at the University of Puerto Rico at Mayagüez campus, several persons and institutions collaborated directly and indirectly with my research. I want to start expressing a sincere acknowledgement to my advisor, Dr. Samuel P. Hernández-Rivera who has trusted and put his faith in me for the last fourteen years and for his invaluable scientific support, guidance and friendship.

I would also like to thank my doctoral committee: Dr. Miguel Castro, Dr. Nairmen Mina, Dr. Luis Rivera, Dr. Julio Briano and Dr. Narinder Mehta for their time and availability to help me during the progress of this research. I would like to thank Mr. Julio Cartagena senior member of technical staff at Hewlett-Packard Caribe, Ltd. for giving me the opportunity of completing the practicum or internship requirement in Aguadilla facilities. Last but not least, I would like to thank Alfred P. Sloan Foundation and Center for Chemical Sensors Development for the financial support.

Table of Contents

List of Symbols and Abbreviations ……....xi

List of Figures ……xiii

List of Tables ……xv

1 INTRODUCTION

1.1 Motivation ……..…..1

1.2 The polymorphism of RDX ……3

1.3 Computational methods ……..……...5

1.3.1 General considerations ……..…….5

1.3.2 Density functional theory ……..…….8

1.3.3 NMR spectral properties ……12

1.3.4 The calculation of the chemical shielding …….……13

1.3.5 Quantum treatment of magnetic shielding ……..…...16

1.3.6 Density functional theory of chemical shifts …..…….20

1.4 Objectives ……21

2 MATERIALS AND METHODS

2.1 Isotopic studies ……..……....23

2.1.1 Labeled RDX's ……..……23

2.1.2 Vibrational spectroscopy ……..……23

2.1.3 Computational methods ……..……24

2.2 α→β phase transition ……24

2.2.1 Preparation of RDX ……..……24

2.2.2 Equipment ……..……..25

2.2.3 Raman spectroscopy ……..……...25

2.2.4 Computational methods ……..……25

2.3 NMR studies of nitramines ……..…...26

2.3.1 NMR measurements ……...26

2.3.2 Computational methods ……..……27

3 VIBRATIONAL SPECTRA AND STRUCTURE OF α-RDX AND ITS ^{13}C AND ^{15}N-LABELLED DERIVATIVES: A THEORETICAL AND EXPERIMENTAL STUDY

3.1 Introduction ……29

3.2 Results ……..31

3.3 Discussion ……...32

4 MONITORING α→β PHASE TRANSITION OF RDX WITH FT-RAMAN SPECTROSCOPY

4.1 Introduction ……40

4.2 Results ……..42

3.3 Discussion ……...46

5 ^{13}C AND ^{15}N NMR CHEMICAL SHIFTS CALCULATIONS ON NITRAMINE SYSTEMS: A COMPARISON OF METHODS AND BASIS SETS

5.1 Introduction ……51

5.2 Results ……..55

5.3 Discussion ……...56

6 CONCLUSIONS ……..……..66

7 REFERENCES ……..69

List of Symbols and Abbreviations

σ	Chemical shielding tensor
AAA	Axial, axial, axial
AAE	Axial, axial, equatorial
ATR	Attenuated total reflectance
$B°$	External magnetic field
B3LYP	Beck three-parameter Lee-Yang-Parr
cc-PVTZ	Correlation consistent polarized valance triple zeta
CSGT	Continuous set of gauge transformations
δ	Chemical shift tensor
DFT	Density functional theory
DMSO	Dimethylsulfoxide
EEE	Equatorial, equatorial, equatorial
E_J	Electron-electron repulsion term
E_T	Kinetic energy
E_V	Potential energy
E_{xc}	Exchange-correlation term
FT	Fourier transform
FTIR	Fourier transform infrared
GIAO	Gauge including atomic orbital
GPa	Giga Pascal
H	Halmitonian
HK	Hohenberg and Kohn

IGAIM	Individual gauges for atoms in molecules
IGLO	Individual gauge for localized orbitals
kcal	kilocalorie
LCAO	Linear combination of atomic orbitals
μ	Nuclear moment
MBT	Many-body perturbation theory
MP2	Møller-Plesset
nm	Nanometers
NMR	Nuclear magnetic resonance
RDX	Royal demolition explosive
VWN	Vosko, Wilk and Nusair local functional
WLS	Wavenumber linear scaling method
$\rho(\vec{r})$	Electronic density distribution
ψ	Wave function

List of Figures

Figures **Page**

1.1 Equilibrium geometry of RDX molecule in the α-polimorph. Legend: carbon, gray; nitrogen, blue; oxygen, red; hydrogen, white ……. 3

1.2 Coordinate system used to illustrate the gauge origin dependence of the chemical shift ……..... 19

3.2 Structures of α-RDX (a); α-$^{13}C_3$RDX (b) and α–$^{15}N_3$RDX (c). * Reference for vibrational analysis ……. 30

3.2 Experimental FTIR spectra for RDX and isotopically labeled RDX from 500 to 1600 cm^{-1}; (a) RDX solid (black); (b) $^{13}C_3$-RDX (red) and (c) $^{15}N_3$-RDX (blue) …… 33

3.3 Experimental FT-Raman spectra for RDX and isotopically labeled RDX from 2800 to 3200 cm^{-1}. (a) RDX solid (black); (b) $^{13}C_3$-RDX (red) and (c) $^{15}N_3$-RDX (blue) …….. 34

3.4 Experimental FT-Raman spectra for RDX and isotopically labeled RDX from 100 to 1700 cm^{-1}. (a) RDX solid (black); (b) $^{13}C_3$-RDX (red) and (c) $^{15}N_3$-RDX (blue) ……..... 35

3.5 Theoretical Raman spectra (B3LYP/6-311+G**) for RDX and isotopically labeled RDX from 100 to 1700 cm^{-1}; (a) RDX normal (black); (b) $^{13}C_3$-RDX (red) and (c) $^{15}N_3$-RDX (blue) ……... 38

4.1 Structures of α-RDX (a), β-RDX (b) and γ-RDX (c) ……..... 41

4.2 Raman spectral changes upon slow heating α-RDX to 204°C and then cooling to room temperature. An α→β-RDX transition occurs. Heating: (a) 25°C; (b) 150°C; (c) 202°C; (d) 204°C. Cooling: (e) 202°C; (f) 150°C; (g) 25°C …… 44

4.3 Effect of temperature on Raman modes in the frequency range 2900-3200 cm^{-1}. Heating: (a) 25°C; (b) 150°C; (c) 202 °C; (d) 204°C. Cooling: (e) 202°C; (f) 150°C; (g) 25°C …… 45

4.4 Theoretical and experimental FT-Raman spectra for RDX and conformers from 100 to 1700 cm^{-1} using B3LYP/6-311++G**: (a) calculated AAE RDX conformer, (b) experimental α-RDX, (c) calculated EEE-RDX conformer, (d) calculated AAA-RDX conformer and (e) experimental β-RDX ……..... 49

5.1 The structures of the investigated nitramines. (1) 1-nitro-1-azaethane (MNA); (2) N,N-dimethylnitramine (DMNA); (3) 1,1-dinitro-1-1-aza-ethane (MDN); (4) N,N-diethylnitroamine (DENA); (5) 1,3-dinitro-1,3-diazacyclobutane (TETRAGEN); (6) 1,1,3-trinitroazetidine (TNAZ): (7) 1,3-dinitro-1,3-diazacyclopentane (CPX); (8) N-nitropiperidine (NP); (9) 1,4-dinitro-1,4-diazacyclohexane (CDNC); (10) Hexahydro-1,3,5-trinitro-s-triazine (RDX)…….. 54

5.2 The linear regression between experimental and theoretical DFT predicted ^{13}C NMR chemical shifts for cyclic and acyclic nitramines using different models and basis set; ○ GIAO/6-311+G(2D,P), ● GIAO/cc-pVTZ, ▲ CSGT/6-311+G(2D,P), ∆ CSGT/ cc-pVTZ …… 62

5.3 Mean absolute error for the ^{13}C (●), ^{15}N-Nitro (○) and ^{15}N-Amine (▲) NMR calculations at different models using different basis set. The geometry optimizations of the structures utilized as inputs were performed at B3LYP/6-311+G(D,P) theory level …… 63

5.4 Solid-state CP/MAS ^{15}N NMR spectrum of RDX …….. 64

List of Tables

Tables **Page**

3.1 Observed, calculated and assigned frequencies of fundamental modes for α-RDX, $^{13}C_3$RDX and $^{15}N_3$RDX isotopomers[a] …….. 39

4.1 Absolute and relative energies of RDX conformers …… 43

4.2 Observed, calculated and assigned frequencies of fundamental modes for α and β-RDX……..…… 50

5.1 ^{13}C and ^{15}N experimental and theoretical chemical shifts for acyclic nitramines at different models and basis set …… 58

5.2 ^{13}C and ^{15}N experimental and theoretical chemical shifts for cyclic nitramines at different models and basis set …… 59

5.3 Slope (a), intercept (b) and linear correlation coefficient (R^2) found for the different combination of model and basis set for ^{13}C and ^{15}N NMR calculations ……..…….. 61

5.4 Mean absolute error (MAE) for the different combination of model and basis set for ^{13}C and ^{15}N NMR calculations …… 61

1 INTRODUCTION

1.1 Motivation

Hexahydro-1,3,5-trinitro-s-triazine or RDX (for Royal Demolition eXplosive) is one of the most widely employed high explosives (HE) in military applications today. The extensive use of RDX is associated to its reasonable insensitivity to external conditions and high performance level. Various experimental and theoretical techniques have been used in order to determine the structure of RDX in the gas, solid and liquid states (Rice and Vladimiroff, 2002; Karpowicz and Brill, 1984; Filhol et al., 1971; Rey-Lafon et al., 1971). Some of the greatest improvements in explosives detection during the last years have been made in the area of vibrational spectroscopy. Several of these methods have been shown capable of detecting explosives on surfaces at stand-off distances, although much work remains to be done to improve selectivity and differentiation from matrix effects and background clutter.

To understand the explosive nature of RDX, the molecular structure needs to be examined in detail. RDX is known to exist in four polymorphic phases, termed α, β, γ and δ (Choi and Prince, 1972; Karpowicz and Brill, 1984; Ciezack et al., 2007; Dreger and Gupta, 2007). The vibrational spectroscopy of α-RDX has been the subject of numerous studies (Rice and Chabalowski, 1997; Castro et al., 2004). However, some inconsistency exists in the available studies of α-RDX, with respect to the assignment of some normal vibrations. Assignments of the IR and Raman bands are made mainly on the basis of empirical comparison

of experimental results with those of related groups such as nitro and amino groups. There are only a few vibrations which are not combination modes involving more than one type of motion. The degree of mixing is evident in the varying amounts of frequency shifts that are observed. In this sense the effects of the ^{13}C and ^{15}N substitution on various vibrations are large enough to be useful in matching calculated and measured frequencies. The infrared and Raman spectra, in solid state, of α-phase and ^{13}C and ^{15}N (on ring) enriched RDX analogues were obtained for the study. Quantum chemical calculations have also been performed, and many vibrational bands have been clearly assigned.

In contrast to the experimental data available for α-phase, there is limited experimental data on the characterization of the solid β-phase. The RDX transition between α and β solid phases occurs at 204 °C and is detectable by changes in the Raman spectra. This temperature-induced phase transition has not been reported previously and may play an important role in the stages of explosive initiation.

In addition, it is a generally accepted idea that nitro groups represent the primary cause of initiation reactivity of polynitro compounds. Recently, relationships between explosive properties (electric spark sensitivities, detonation and thermal decomposition) and ^{15}N NMR chemical shifts of nitrogen atoms of nitramino groups were reported. In the present study, two theoretical models with different basis set were applied to predict NMR shielding tensor for RDX and others cyclic and acyclic nitramine systems and were compared with experimental results.

All experimental results were supported by performing density functional theory (DFT) (Kohn et al., 1996) calculations for energies, geometries, vibrational frequencies and shieldings constants. The theoretical data have satisfactorily reproduced experimental results and DFT offers an acceptable trade off between accuracy and speed.

1.2 The polymorphism of RDX

The RDX molecule consists of the three NO_2 groups bonded to the nitrogen atoms of a triazine ring (see Figure 1.1). The conformers of RDX are distinguished mainly by the arrangement of nitro groups relative to the rings atoms of the RDX molecule. In the solid state, RDX is known to exist in four polymorphs: α, β, γ andδ.

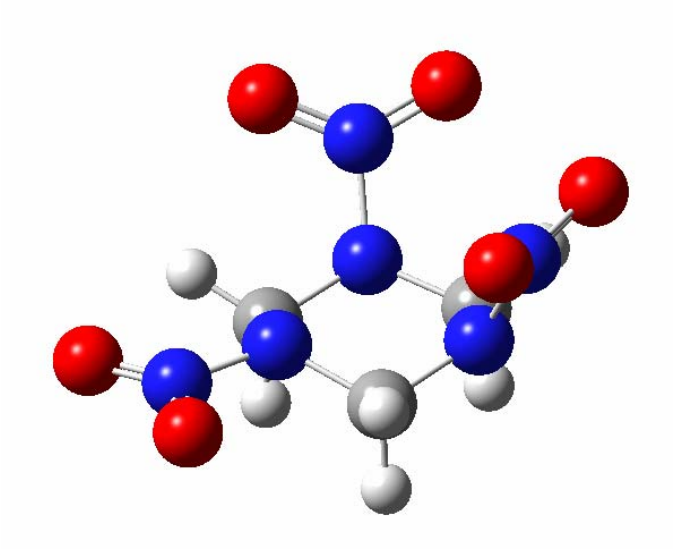

Figure 1.1 Equilibrium geometry of RDX molecule in the α-polymorph.
Legend: carbon, gray; nitrogen, blue; oxygen, red; hydrogen, white.

The α-polymorph exists at ambient conditions and has an orthorhombic structure belonging to the Pbca space group with eight molecules per unit cell (Choi and Prince, 1972). All molecules occupy sites of C_1 symmetry, but they possess C_s pseudo-symmetry with two of the nitro groups in the axial (A) position with respect to the s-triazine ring and the third in an equatorial (E) position. This molecular conformation is usually referred to as the chair AAE conformer.

A second polymorph of RDX, labeled β-RDX, is obtained either by evaporation of boiling solvent containing RDX (Brill et al., 1983), deposition of RDX from solution on a glass substrate (Castro et al., 2004), or under high temperature and high pressure (Miller et al., 1991). On the basis of comparison between the vibrational spectra of the β-polymorph and that of RDX in the gas phase and in solution, the molecular symmetry for this polymorph was suggested to be C_{3v}. Further experimental and theoretical studies (Harris and Lammertsma, 1997; Rice and Chabalowski, 1997) for the gas phase showed that the C_{3v} conformer may assume a structure in which all of the NO_2 groups are in axial positions with respect to the s-triazine ring, forming the so-called AAA conformation.

The γ-polymorph was observed under high pressure above 3.8 GPa, using X-ray diffraction (Yoo et al., 1998), by Raman spectroscopy (Baer et al., 1990) and IR spectroscopy (Goto et al., 2006). Symmetry correlation analyses indicate that the γ-polymorph may assume one of the three orthorhombic structures: D_{2h}, C_{2v} or D_2. On the basis of the available X-ray data, the D_{2h} factor group is favored over the other structures, and it is proposed that γ-phase RDX has a space group

isomorphous with a point group D_{2h} with eight molecules occupying the C_1 symmetry sites, similar to the α-phase.

The γ-RDX phase remains kinetically stable in the pressure range between 17.8 and 18.9 GPa where prominent discontinuities in the frequency shifts suggest the existence of another new phase (δ) (Dreger and Gupta, 2007). The δ-phase has vibrational characteristics that are similar to those of β-RDX, suggesting the two polymorphs share a related crystal structure.

1.3 Computational Methods

1.3.1 General considerations

It is now possible to describe molecular properties of relative small molecules with nearly chemical accuracy using theoretical methods due to recent advances in computational methods and common access to large-scale powerful computers and software. The application of quantum mechanical calculations to energetic materials has expanded dramatically. Two major classes of electronic structure methods have been devised and are frequently used in the literature; semi-empirical methods and *ab initio* methods. The development of semi-empirical methods gained popularity in the 1970s-1980s. These methods use derived parameters from experimental data to fit into the computations. Semi-empirical calculations continue to appear in large numbers in the chemical literature. Since there will always be researchers interested in molecules that exceed the size of those practically accessible by *ab initio* methods, semi-

empirical levels of molecular orbital theory are certain to continue to be developed and applied (Cramer, 2004). The fundamental assumption of Hartree-Fock (HF) theory (Henre et al., 1986), that each electron sees all of the others as an average field, allows for tremendous progress to be made in carrying out practical molecular orbital calculations. However, neglecting electron correlation can have profound chemical consequences when it comes to determining accurate wave functions and properties derived there from. The development of semi-empirical theories was motivated in part by the hope that judicious parameterization efforts could compensate this feature of HF theory. While such compensation has no rigorous foundation, to the extent that it allows making accurate chemical predictions, it may have great practical utility. Early developers of so-called '*ab initio*' (Latin for 'from the beginning') HF theory, however, tended to be less focused in making short-term predictions, and more focused on long-term development of a rigorous methodology that would be worth the wait. The ultimate goal is to solve Schrödinger's equation, which cannot be solved in a practical sense for all but the most simple of systems. To that extent, an enormous amount of effort has been spent on developing mathematical and computational techniques to reach the HF limit, which means to solve the HF equations with the equivalent of an infinite basis set, with no additional approximations. Initially *ab initio* methods were limited to small systems e.g. hydrogen. Often, the implementation of these methods takes a significant amount of computer capabilities and are memory consuming. Thus, only systems with relatively few atoms can be computed within reasonable time. Properties such as

total energies, charge distributions, reaction pathways and vibrational frequencies are often comparable to experimental observables. With the development of faster computers, calculations can be made for large systems and physico-chemical information can be derived.

Since the 1980s, density functional theory (DFT; Kohn et al., 1996) has emerged as a useful method for quantum chemical studies since it is computationally less intensive and includes electron correlation effects. For the 'average' problem, DFT is the method of choice to achieve a particular level of accuracy at lowest computational expenditure. With the appearance of each new functional, there has tended to be at least one paper benchmarking the performance of that functional on a variety of standard test sets (for energies, structures, etc.) and there is now a rather large body of data that is somewhat scattered and disconnected with respect to individual functional performance. Among modern functionals, B3LYP has proven to be the most popular to date. Excellent in-depth texts such as "Essentials of Computational Chemistry" by Cramer (Cramer, 2004) provide commendable coverage on the strengths and weaknesses of DFT. Some of the experimental results presented in this thesis have an important theoretical support by means of DFT calculations. The next section is devoted to briefly introduce the basic concepts, we have used throughout the present work.

1.3.2 Density functional theory (DFT)

The Density Functional Theory (DFT) approach is based upon a strategy of modeling electron correlation via general functionals of the electron density. A functional is a function whose argument definition is itself a function: in other words, a function of a function. DFT is primarily a theory of electronic ground state structure, couched in terms of the electronic density distribution $\rho(\vec{r})$. DFT is an alternative and complementary, approach to the traditional methods of quantum chemistry which are couched in terms of the many-electron wave function $\Psi(r_1....r_N)$. The starting point of DFT is the rigorous, simple lemma of Hohenberg and Kohn (H-K; Hohenberg and Kohn, 1964). In the language of DFT, the ground state properties of an interacting electron gas could be calculated from the electron density $\rho(\vec{r})$, independent of the external potential. The electron density distribution $\rho(\vec{r})$ is composed of three spatial variables. The electronic state, the energy and all the electronic properties of a system could be uniquely described in terms of this $\rho(\vec{r})$ as shown in equation 1.1

$$\rho(\vec{r}) = N.\int ...\int \left|\psi(\vec{x}_1, \vec{x}_2, ...\vec{x}_n\right|^2 ds_1 d\vec{x}_2 .....d\vec{x}_n \qquad (1.1)$$

$\rho(\vec{r})$ determines the probability of finding any of the N electrons within the volume element $d\vec{r}_1$ (with an arbitrary spin). The dependence on total number of electrons immediately suggests that a useful physical observable would be the

electron density ρ, since, integrated over all space, it gives the total number of electrons N.

The basic properties of the electron density are:

$$\rho(\vec{r} \to \infty) = 0 \tag{1.2}$$

$$\int \rho(\vec{r}) d\vec{r} = N \tag{1.3}$$

Moreover, because the nuclei are effectively point charges, it should be obvious that their positions correspond to local maxima in the electron density, so the only issue left to completely specify the Hamiltonian is the assignment of nuclear atomic numbers. It can be shown that this information is also available from the density, since for each nucleus A located at an electron density maximum r_A,

$$\left.\frac{\partial \overline{\rho}(r_A)}{\partial r_A}\right|_{rA=0} = -2Z_A \rho(r_A) \tag{1.4}$$

where Z is the atomic number of A, r_A is the radial distance from A, and ρ is the spherically averaged density. The arguments above do not provide any simpler *formalism* for finding the energy. They simply indicate that given a known density, one could solve the Schrödinger equation form the Hamiltonian operator and determine the wave functions and energy eigenvalues. As previously noted, to establish a dependence of the energy on the density, and in the Hohenberg–Kohn (H-K) theorem it is the ground-state density that is employed. It is sufficient to show that this density determines the Hamiltonian operator and thence, implicitly, all properties determined by H. The Hohenberg-Kohn theorem basically establishes that there is one–to-one mapping between the ground state electronic density and the ground state wave function. Therefore, the calculation

of the density can be replaced by a calculation of the wave function which defines the system. The Hohenberg-Kohn theorem demonstrated the existence of a unique functional which determines the ground state energy and density exactly but does not provide the form of this functional. The H-K theorem does not tell us what the true total energy functional is; only that it exists.

The most common implementation of density functional theory is through the Kohn-Sham method (Kohn W. and Sham L. J. 1965), which maps the properties of the system onto the properties of a system containing non-interacting electrons under a different potential. In the Kohn-Sham equations, the interaction among electrons is simulated via an effective potential due to the surrounding electrons. Within the framework of Kohn-Sham method, the approximate functionals employed by the current DFT methods partitions the electronic energy into several terms:

$$E = E_T + E_V + E_J + E_{XC} \tag{1.5}$$

where E_T is the kinetic energy term, E_V includes terms describing the potential energy of the nuclear-electron attraction and of the repulsion between pairs of nuclei, E_J is the electron-electron repulsion term and E_{XC} is the exchange-correlation term and includes the remaining part of the electron-electron interactions. All terms, except the nuclear-nuclear repulsion, are functions of ρ, the electron density. The energy sum: $E_T + E_V + E_J$, corresponds to the classical energy of the charge distribution ρ. The E_{XC} term is determined entirely by the electron density and is usually divided into separate parts, referred to as the

exchange and correlation parts, but actually corresponding to same-spin and mixed-spin interactions respectively.

$$E^{XC}(\rho) = E^{X}(\rho) + E^{C}(\rho) \tag{1.6}$$

All the three terms are again functionals of the electron density, and functionals defining the two components on the right side of equation 1.6 are termed exchange functionals and correlation functionals, respectively. Since no exact functionals for exchange and correlation are known (except for the free electron gas) some approximations have to be included in order to calculate physical quantities. Basically, two approximations are used in DFT: the local-density approximation (LDA) (Becke, 1993) and generalized gradient approximation (GGA). In physics, the most widely used approximation is the LDA, where the functional depends only on the density at the coordinate where the functional is evaluated. The GGA functionals are still local, but also take into account the gradient of the density at the same coordinate. Difficulties in expressing the exchange part of the energy can be relieved by including a component of the exact exchange energy calculated from Hartree-Fock theory. Functionals of this type are known as hybrid functionals. Of all modern hybrid functionals, B3LYP has proven the most popular today. Its overall performance is remarkably good for geometries and frequency calculations and is not an expensive method.

The exchange-correlation for a hybrid functional is usually a linear combination of the Hartree-Fock exchange (E_X^{HF}) and some combination of

exchange and correlation functionals. The parameters relating the amount of each functional can be arbitrarily assigned and is usually fitted to reproduce well some set of observables (bond lengths, band gaps, etc). The popular, three parameters Becke B3LYP exchange-correlation functional (Becke, 1988; Lee-Yang-Parr, 1988; Kim et al., 1994; Stephens et al., 1994) is defined by:

$$E_{XC}^{B3LYP} = E_{XC}^{LDA} + a_0(E_X^{HF} - E_X^{LDA}) + a_X(E_X^{GCA} - E_X^{LDA}) + a_C(E_X^{GCA} - E_X^{LDA}) \quad (1.7)$$

where $a_0 = 0.20$, $a_X = 0.72$ and $a_C = 0.81$ are the three empirical parameters; E_X^{GGA} and E_C^{GGA} are the generalized gradient approximation formulated with the Becke 88 exchange functional (Becke, 1988) and the correlation functional of Lee, Yang and Parr (Lee C. et al., 1988), and E_C^{LDA} is the Vosko, Wilk and Nusair (VWN) local functional (Vosko, et al., 1980).

The formal scaling behavior of DFT has already been noted to be in principle no worse than N^3, where N is the number of basis functions used to represent the Kohn-Sham orbitals. This is better than HF by a factor of N, and substantially better than other methods that, like DFT, also include electron correlation.

1.3.3 NMR spectral properties

Nuclear magnetic resonance (NMR) is probably the most widely applied spectroscopic technique in modern chemical research. Its high sensitivity and the mild conditions required for its application render it peerless for structure determination and kinetics measurements in many instances. As an experimental

technique, its use is extraordinarily widespread. Until quite recently, however, theoretical prediction of NMR spectral properties significantly lagged experimental work. The ultimate factor slowing theoretical work has been simply that it is more difficult to model the interactions of a wave function with a magnetic field than it is to model interactions with an electric field (Facceli, 2004). The inclusion of a magnetic field *B* in the Hamiltonian is achieved by the minimal substitution which includes the vector potential **A**. The vector potential **A** uniquely determines the magnetic field *B* through *B* = rot **A**. However, there is no unique choice of the vector potential A for a given magnetic field B. The freedom in the choice of the gauge origin should have no consequences since all physical quantities are requested to be gauge-invariant. However, gauge-invariance holds only for exact solutions to the Schrödinger equation and cannot be enforced for approximations wavefunctions. It turns out that the source of the gauge origin problem in quantum chemistry is the finite basis set representation of the wavefunctions. Nevertheless, significant progress has been made over the last decade, particularly with respect to DFT, and calculation of chemical shifts is becoming much more of a routine than had previously been. This section begins with a very brief summary of some of the technical issues associated with NMR spectral calculations. Subsequent subsections address the various utilities of modern methods for predicting chemical shifts.

1.3.4 The calculation of the chemical shielding.

A nucleus with a non-zero nuclear magnetic moment μ provides an excellent probe of the magnetic fields inside a sample. Exposed to a static homogeneous magnetic field, the nuclear magnetic moment will precess around the direction of the magnetic field with a frequency directly proportional to the magnitude of the magnetic field. The frequency and thus the magnetic field at the nuclear site can be detected by nuclear magnetic resonance (NMR) experiments. This introduced magnetic field, B_A^1 at the nucleus A, is opposite in the direction to the applied external magnetic field and is proportional to the magnitude of B^0, according to Lenz Law. So the magnitude of the magnitude of the magnetic field at nucleus A can be expressed as

$$B_A = B^0 - B_A^1 = B^0(1-\sigma_A) \tag{1.8}$$

where the proportionality constant σ_A is called the shielding constant for nucleus A. The ability of the applied field to induce a current in the molecule, and hence the strength of the resulting local magnetic field experienced by nucleus, depends on the details of the electronic structure near magnetic nucleus of interest, so nuclei in different chemical groups have different shielding constants. For that reason NMR spectroscopy has become a standard tool to characterize chemically different sites of an ion in a molecule or in a crystal.

There is considerable confusion in the literature about the use of the terms: “chemical shift” and “chemical shielding” (Facceli, 2004). The chemical shielding is the tensor that describes the relative change in the local magnetic field at the nucleus position relative to external magnetic field. In general,

shielding effects are associated with diamagnetic effects from spherical charge distribution, whereas de-shielding effects are associated with a nonspherical charge distribution originating from *p* or higher angular momentum electrons. In practice, NMR experiments do not measure the chemical shielding directly; instead, the common practice is to measure the chemical shifts as the change of resonance frequency of a nucleus relative to a given standard. The formal relation between the chemical shift and chemical shielding tensors is given by

$$\delta = 1\sigma_{iso} - \sigma \tag{1.9}$$

where δ is the chemical shift tensor, σ is the chemical shielding tensor, 1 is the unit matrix, and σ_{iso} is the isotropic value or trace of the chemical shielding of the standard reference used in NMR experiments.

There are several scientific reasons to pursue research efforts in calculating chemical shielding, but one of the most common applications is associated to the chemical shielding dependence on the molecular geometry and specific chemical environment. A common difficulty in the calculation of magnetic properties is that the usual wave functions do not guarantee gauge invariance, i.e., in the simplest case, the results may depend on the position of the molecule in the Cartesian coordinate frame. The physical reason for this is that a magnetic field, say in the *z* direction, leads to a perturbation *in the momenta*, which twists the molecular orbitals around the *z* axis in the imaginary *xy* plane. If an atom is situated on the z axis, its basis set is close under this rotation, and it can be described equally well both unperturbed state and in the presence of the

perturbation. However, for an atom far from the z axis, the rotation of the orbitals can only be described by using high angular momentum basis functions, which are not normally included in the basis set.

More satisfying solutions to the gauge-origin problem have been offered by approaches which introduce local gauge origins to define the vector potential; an idea which originates in London's study of the molecular diamagnetism more than 60 years ago. Within quantum chemical NMR shift calculation, this idea was first adopted by Ditchfield in his gauge including atomic orbital (GIAO) method (Ditchfield, 1974), in which each atomic orbital has its own local gauge origin placed on its center. The most common methods, in addition to the GIAO's approach, are IGLO, individual gauge for localized orbitals (Schindler M. and Kutzelning, 1982); LORG, localized orbitals local origin (Bouman and Hansen, 1989), IGAIM, individual gauges for atoms in molecules (Keith and Bader, 1992) and CSGT, continuous set of gauge transformation (Keith and Bader, 1993). The GIAO method is generally preferred in the modern literature because it is free of localization artifacts and appears to be less sensitive to basis set quality (Gabor and Pulay, 2003).

1.3.5 Quantum treatment of magnetic shielding

The interaction of an external magnetic field B^0 with a nuclear magnetic moment μ_A inside a molecule, as observed in nuclear magnetic resonance, can be described by the Zeeman energy change,

$$\Delta E = -\mu_A \cdot B \tag{1.10}$$

where B is effective magnetic field felt by the nuclear moment. This effective magnetic field arises because the electrons are influenced by the external magnetic field and give rise to an induced magnetic field at the site of nucleus A,

$$B_i^1 = -\sigma_{ij}^A B_j^0 \tag{1.11}$$

where σ_{ij}^A is called the shielding tensor of nucleus A.

$$\Delta E = -\mu_A \cdot B^0 + \mu_A \cdot \hat{\sigma}^A \cdot B^0 \tag{1.12}$$

where the first term describes the direct interaction between the external magnetic field and the nuclear moment and the second term describes the electron coupled interaction which may be written as a second-order energy change,

$$\sigma_{ij}^A = \left[\frac{\partial^2 E(B^0, \mu_A)}{\partial B_i^0 \partial \mu_{Aj}} \right]_{\mu_A = B^0 = 0} \tag{1.13}$$

arising from a consideration of the energy of a molecule in the presence of an external magnetic field and a perturbing nuclear moment μ_A.

In the Hartree-Fock method, the electronic energy of a molecule in the presence of the external magnetic field B^0 and the nuclear moment μ_A is given as the expectation value of the appropriate Hamiltonian operator using a single determinant wave function. In terms of the doubly occupied molecular Ψ_i, this expression is

$$E(B^0,\mu_A)=\sum_{i=1}^{N/2}2\left\langle\psi_i\left|\hat{h}\right|\psi_i\right\rangle+\left\langle\psi_i\left|\hat{g}\right|\psi_i\right\rangle \tag{1.14}$$

where the one-electron Hamiltonian operator, $\hat{h}$ is

$$\hat{h}=\frac{1}{2m}\left[-i\hbar\nabla+\frac{e}{c}A\right]^2-\sum_k^{atoms}\frac{e^2Z_k}{|r_k|} \tag{1.15}$$

and $\hat{g}$ is the two-electron Hamiltonian operator. In equation 1.15, the vector potential *A* is

$$A=\frac{1}{2}B^0\times r+\frac{\mu_A\times r_A}{|r_A|^3} \tag{1.16}$$

and is due to the uniform external magnetic field B^0 and the magnetic moment of nucleus A, i.e. μ_A. The number of electrons is N and Z_k is the charge of the kth nucleus. The vectors r and r_k are the distance vectors of the coordinate system and nucleus k, respectively. Figure 1.2 shows a coordinate system used to illustrate the gauge origin dependence of the chemical shielding. O is the origin of coordinates, O' is the new origin, $R_{O'}$ is the position of the new origin of coordinates with respect to original one, R_A is the position of the nucleus A, r_k is the position of the electron with respect to O, r_{Ak} is the position of the electron with respect to the nucleus A, and r'_k is the position of the electron relative to the new origin of coordinates O'.

With GIAO, the molecular orbitals, ψ_i, are still expressed as a linear combination of atomic orbitals (LCAO), ϕ_μ^0, as in the Hartree-Fock method, that is,

$$\psi_i = \sum_{\mu}^{m} c_{\mu i} \phi_\mu \tag{1.17}$$

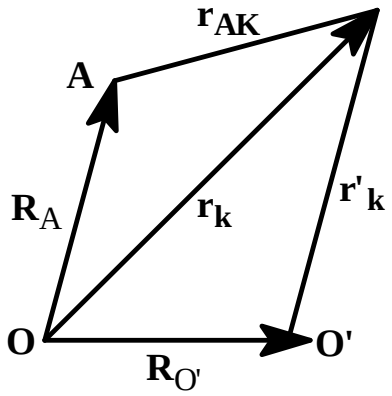

Figure 1.2 Coordinate system used to illustrate the gauge origin dependence of the chemical shift.

where *m* is the total number of the basis functions. But the atomic orbitals (basis functions) used here are not same those used in the ordinary Hartree-Fock method. The relationship between the basis functions, ϕ_μ, used in the GIAO method and the basis functions, ϕ_μ^0, used in the ordinary Hartree-Fock method is

$$\phi_\mu = f_\mu \phi_\mu^0 \tag{1.18}$$

and f_μ is the gauge factor and defined as

$$f_\mu = \exp\left(-\frac{ie}{\hbar c} A_\mu r_\mu \right) \tag{1.19}$$

where the vector potential A_μ is

$$A_\mu = \frac{1}{2} B^0 \times R_\mu \tag{1.20}$$

and a new vector R_ν that represents the distance vector from the arbitrary origin of the molecular coordinate system to the atom on which the basis function ϕ_μ is located. Now the total chemical shielding is invariant under changes of the origin of coordinates. In the language of electromagnetic interactions this is equivalent to say that chemical shielding tensor is invariant under gauge transformation which preserve $\nabla \cdot A = 0$.

1.3.6 Density functional theory of chemical shifts

The methods for calculating chemical shieldings that include contributions of the electronic correlation into many-body perturbation theory (MBPT) and coupled-cluster methods do not provide a practical alternative to calculate chemical shieldings because they scale as N^5 to N^7, depending on the approximation, with the number of electrons N in the molecule. Using DFT theory, which scales as N^2, makes possible to calculate chemical shieldings in molecular system of practical interest including electronic correlation effects.

Two important observations derived from results of calculated chemical shifts for different exchange correlation functionals (Cheeseman, et al. 1996): the calculations are not sensitive to the exchange-correlation functional used, except for the LDA approximation and DFT methods recover a significant portion of the electronic correlation effect and provide a viable alternative to calculate chemical shifts with accuracies close to those obtained with the much more

computationally expensive Møller-Plesset 2 method (MP2; Gauss and Stanton, 2002).

1.4 Objectives

Characteristics of high explosives, such as performance, sensitivity and stability, are determined by molecular level properties. These properties have implications for safety and handling as well as the practical use of these explosives materials. Vibrational spectroscopy (IR and Raman) and NMR techniques are widely used to structural and dynamic aspects of molecular systems. Some of the greatest improvements in explosive detection during the past five years have been made in the area of vibrational spectroscopy. This study is part of a comprehensive effort to investigate the molecular conformations of RDX using vibrational spectroscopy and NMR methods. The combination of quantum calculations of chemical shifts and harmonic vibrations with NMR and IR/Raman parameters, respectively, has become an accepted technique to gather insight into molecular structure. Therefore, an understanding of RDX polymorphisms is required for the proper characterization of the reactive behavior of explosive molecular solids. The purpose of our work was fourfold:

1) To assign the fundamental vibration frequencies and to elucidate both force field and structure of α-RDX molecule on the basis of IR and Raman spectra , isotope labeling, and *ab initio* force field calculations.

2) To record ^{1}H, ^{13}C and ^{15}N nuclear magnetic resonance (NMR) spectra in solution and solid state for the RDX and predict the nuclear magnetic resonance (NMR) shielding constants using the gauge independent atomic orbital (GIAO) approach at DFT approach for RDX conformers. We have also extended these studies to other cyclic and acyclic nitramines.

3) To follow temperature-induced structural transformation of α-RDX using Raman spectroscopy and to examine changes in vibrational modes associated with phases transitions.

4) To correlate the experimental and theoretical results and to determine the importance of the qualitative agreement between the experimental and calculated values of the chemical shifts and vibrational analysis in order to enhance the understanding of the molecular structure of RDX conformers.

2 MATERIALS AND METHODS

2.1 Isotopic studies

2.1.1 Labeled RDXs

RDX standards were obtained as 1 mg/mL solution in acetonitrile from Supelco® (Sigma-Aldrich Chemical Co., Milwaukee, WI), ^{13}C (99%) enriched RDX was obtained from Cambridge Isotope Laboratories, Inc. (Andover, MA) as 1 mg/mL acetonitrile solution and ^{15}N (99%) enriched RDX was obtained from SRI International as solid material. Acetonitrile (Sigma-Aldrich) was allowed to evaporate at room temperature after the deposition on metallic slide.

2.1.2 Vibrational spectroscopy

Fourier transform infrared (FTIR) spectra were obtained by attenuated total reflection (ATR) method in a Nexus 8700, Thermo Nicolet FTIR spectrometer in the range of 400-4000 cm^{-1}. Samples were lightly ground in preparation for placement on the ATR stage. Raman spectra were measured using a commercial Renishaw RM2000 Raman microspectrometer with vibrational and white light imaging capabilities. The 514.5 nm line of a Coherent INNOVA 308 Ar+ ion laser system was used as the excitation source. Dispersive Raman equipment was operated in confocal mode microscopy. Spectrometers were equipped with polarization analyzers and de-scramblers. All of measurements were taken at room temperature (ca. 20 °C).

2.1.3 Computational methods

Ab initio density functional theory (DFT) with the B3LYP hybrid functional calculations using the Gaussian 03-W program package (Frisch et al., 2003) were carried out for the α-RDX and its ^{13}C and ^{15}N isotopomers. The basis sets implemented in the program were employed without modification. The hybrid density functional B3LYP method (Lee et al., 1988) was used for geometry optimization and frequency intensity calculations. In all cases, the 6-311++G** basis set was used. Frequencies for isotopically labeled RDX were recalculated following mass substitution using the force constants obtained for the most common isotope. Detailed assignment was given based on the comparison between the theoretical data and the experimental results. The normal mode descriptions were obtained with the assistance of animated pictures based on the normal coordinates.

2.2 α→β phase transition

2.2.1 Preparation of RDX

RDX was synthesized by the Bachmann method (Bachman and Sheena, 1954) with some modifications. Product was purified by recrystallization from acetone. The purity was confirmed with high performance liquid chromatography.

2.2.2 Equipment

The equipment and techniques employed during the slow heating experiment were developed in our laboratory and involved a modified melt-temp apparatus coupled to digital thermometer. The sample was placed in a small hole in the melt-temp and covered with a glass slide. The temperature of the sample was controlled by adjusting the voltage control. The overall heating rate during the controlled experiment (slow heating) was limited to less than 4°C/ min. The temperature of the sample was allowed to equilibrate at a particular temperature for a 3 min before the Raman spectra was recorded. Low setting is adjusted to achieve the temperature rise of 1°C/ minute near the transition temperature. The laser beam has no noticeable effect on these temperatures.

2.2.3 Raman spectroscopy

For the measurement of the Raman spectra a Renishaw RM2000 microspectrometer was used in the 500-3500 cm^{-1} region with 0.5 cm^{-1} resolution. The spectra were excited with a Coherent INNOVA 308 Ar+ ion laser at wavelength 514.5 nm. Samples were held on the variable temperature equipment in their normal crystalline condition.

2.2.4 Computational methods

Density functional theory (DFT) with the B3LYP hybrid functional calculations using the Gaussian 03-W program package (Frisch et al., 2003)

were carried out for the AAE, AAA and EEE-RDX polymorphs. The basis sets implemented in the program were employed without modification. Absolute, relative and zero-points energy of each conformer were established. The hybrid density functional B3LYP method (Lee et al., 1988) was used for geometry optimization and frequencies calculations. In all cases, the 6-311++G(d,p) basis set was used. The problem of overestimation associated to DFT calculations were solved using wavenumber-linear scale method (WLS) (Hiroshi and Akito, 2000). Detailed assignment was given based on the comparison between the theoretical data and the experimental results. The normal mode descriptions were obtained with the assistance of animated pictures based on the normal coordinates using the software GaussView 03 (Frisch et al., 2003).

2.3 NMR studies of nitramines

2.3.1 NMR measurements

All NMR measurements were performed using on Bruker 500 spectrometers system MHz and Varian 300 MHz spectrometers. Samples were examined in DMSO-d_6 solutions and compared with previous acetone-d_6 solution results [Infante and Hernández, 2006). The solvent signal, calibrated against Me_4Si, was used as a reference for proton and carbon-13 spectra. The ^{15}N chemical shifts were referenced to the signal of an external CH_3NO_2. ^{13}C(99%) enriched RDX was obtained from Cambridge Isotope Laboratories, Inc. (Andover, MA) as 1mg/mL acetonitrile solution and ^{15}N (99%) enriched RDX was

obtained from Dr. Ronald Spanggord, SRI, Menlo Park, CA., as solid material. Solid-state CP/MAS (cross-polarization/magic angle spinning) ^{15}N NMR spectra were obtained from Dr. Kevin Thorn, U.S. Geological Survey and were recorded on a Chemagnetics CMX-200 spectrometer at nitrogen resonant frequency of 20.27 MHz. Acquisition parameters included a 2.0 ms contact time, pulse delay of 0.5 s and spinning rate of 5 kHz. The ^{13}C and ^{15}N NMR chemical shifts for some nitramines were taken from literature (Bulusu, 1982; Zeman, 1999). The ^{15}N NMR chemical shift for substances not yet synthesized has been predicted and reported (Zeman, 2006).

2.3.2 Computational methods

GAUSSIAN 03 software package was used for all theoretical calculations. All the molecular geometries were optimized at B3LYP/6-311+(d,p) level, which can give a good geometry at relative low cost. The calculations of NMR shielding tensors were done at B3LYP level of theory using GIAO and CSGT models, using as input the structure optimized at B3LYP/6-311+G(d,p) level. Two basis set were applied to perform these calculations, one of them is the standard Pople style basis sets 6-311+G(2d,p) (Pople et al., 1984), which is a triple split valance with one additional diffuse sp-function, and two d-functions on heavy atoms and one p-function on hydrogen atoms. The other basis set which tested was cc-pVTZ (correlation consistent polarized valance triple zeta) (Dunning and Woon, 1995) which gave good results in describing the effect of a strong electron-withdrawing group (NO_2) in the NMR shielding tensor (Tormena and da Silva,

2004). The chemical shifts were calculated against the shielding of appropriate nuclei in the reference molecule calculated in the same solvent, basis set and method: $\delta_i = \sigma_{ref} - \sigma_i$

3 VIBRATIONAL SPECTRA AND STRUCTURE OF α-RDX AND ITS ^{13}C AND ^{15}N-LABELLED DERIVATIVES: A THEORETICAL AND EXPERIMENTAL STUDY

3.1 Introduction

The cyclic nitramine hexahydro-1,3,5-trinitro-*s*-triazine (RDX) is a well-known powerful secondary explosive that has attracted considerable attention due to its physical properties. The trinitrate ester is very persistent in the environment with an estimated lifetime of 90 years, under varied soil conditions. Another property that has been the subject of several investigations is the possible conformational arrangements that lead to polymorphism in RDX. The conformers of RDX are distinguished mainly by the arrangement of nitro groups relative to the rings atoms of the RDX molecule. The α-form, shown in Figure 3.1, is the stable polymorph at room temperature and is used in the general bulk level applications. The individual α-RDX molecules possess essentially C_s symmetry with two of the NO_2 groups axial and the third equatorial with respect to the triazine ring. In the present study we have reinvestigated the structure and vibrational spectra of solid α-RDX and its ^{13}C and ^{15}N isotopomers. The structures of the three molecular spatial arrangements (isotopomers) are shown in Figure 3.1. Trace explosive detection is a major technological challenge. The most promising and sensitive devices and techniques for explosive detection that provide qualitative and quantitative information are not amenable to routine field use. IR and Raman spectrometry promise to perform well as portable fieldable parts of an explosive detection system for identifying or confirming the presence

of hidden explosives. The techniques can also be adapted for standoff detection. Some of the greatest improvements in explosives detection have been made in the area of vibrational spectroscopy. The interest in terahertz spectroscopy for explosive detection has robustly increased (Huang et al., 2004).

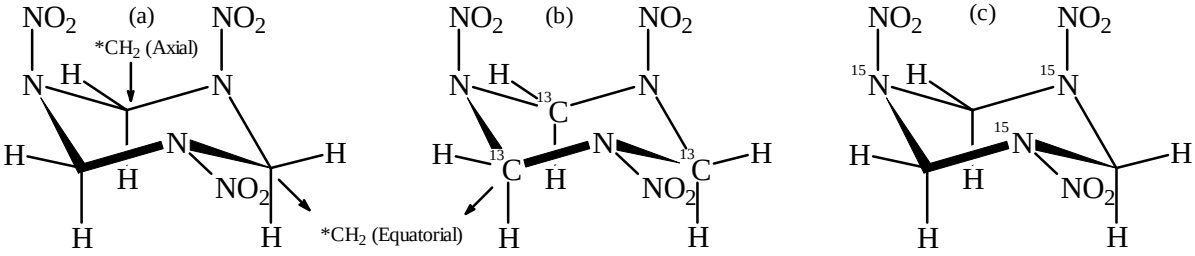

Figure 3.1 Structures of (a) α-RDX; (b) α-$^{13}C_3$RDX; and (c) α–$^{15}N_3$RDX.
* Reference for vibrational analysis.

The new terahertz technology and methods for real-time chemical specific explosive detection were recently developed and presented at SPIE conferences. Interpretation of IR, Raman and Terahertz data, however, required detailed knowledge of the structure and vibrational modes of the molecule examined. The vibrational spectroscopy of RDX has been the subject of numerous studies (Rice and Vladimiroff, 2002; Karpowicz and Brill, 1984; Filhol et al., 1971; Rey-Lafon et al., 1971; Rice and Chabalowski, 1997; Castro et al., 2004). Some inconsistency, however, exists in the available studies of RDX, with respect to the assignment of some normal vibrations. Assignments of the IR and Raman bands are made mainly on the basis of empirical comparison of experimental results with those of related groups such as nitro and amino groups. This work

focuses on the use of modern density functional theory (DFT) (Kohn et al., 1996), to account for the experimental vibrational Raman and IR data from RDX and its ^{13}C and ^{15}N-RDX isotopomers. Raman and IR frequencies were calculated at the DFT/B3LYP level using the 6-311++G** basis set. The calculated frequencies were compared with the experimental data and the isotopic effects are discussed. Assignments of the vibrational modes for RDX are made through comparison between experimental and density functional calculations results. The purpose of the present study is to assign the fundamental vibrational frequencies, to elucidate the structure of RDX, and to analyze the force field on the basis of IR and Raman spectra including isotopic labeling and *ab initio* force field calculations.

3.2 Results

Experimental Raman and FTIR solid phase spectra of α-RDX and its isotopically labeled $^{13}C_3$-RDX and $^{15}N_3$-RDX are shown in Figures 3.2 and 3.3. The spectra of RDX and its isotopic analogues are characterized by intense and sharp vibrational bands. Solid α-RDX has close to C_s symmetry and occupies a C1 site. The 57 fundamental vibrational modes are active in both IR and Raman. These modes included 26 planar modes with A' symmetry and 31 non-planar modes with A" symmetry. Several of these are not expected to be detected because they are either too weak or appear below the limit of detection in this study. The assignments for the IR and Raman frequencies of α-RDX and its

isotopomers, together with the results of the B3LYP calculations are listed in Table 1. The problem of the overestimation commonly encountered in DFT vibrational frequencies calculations due to the neglecting of anharmonicity effects, was solved using a wavenumber-linear scaling (WLS) method (Hiroshi and Akito, 2000) with the following relationship:

$$\nu_{obs} / \nu_{calc} = 1.0087(9) - 0.0000163(6)(\nu_{calc} / cm^{-1}) \quad (3.1)$$

All assignments were determined by comparison of experimental shifted data of the labeled RDX with the calculated wavenumbers and vibrational modes at each selected mode. There are some differences of wavenumbers between calculated and experimental data. This is because the calculated spectra correspond to the gas phase whereas experimental data are taken with solid RDX. However, the spectral patterns are similar. The simulated Raman spectra of RDX for all isotopic are shown in Figure 3.4.

3.3 Discussion

The assignments of selected normal vibrations of the RDX, $^{13}C_3$-RDX and $^{15}N_3$-RDX isotopomers are presented in Table 1, listing the experimental and the calculated frequencies. The calculation gives a reasonable prediction of the normal mode frequencies and the observed isotopic shifts. The normal harmonic frequencies tend to become smaller with increasing isotopic mass, and intensity sometimes changes. From Figures 3.3 and 3.4, it may be said that the principal

features of the observed Raman spectrum are satisfactorily reproduced by the quantum chemical calculations.

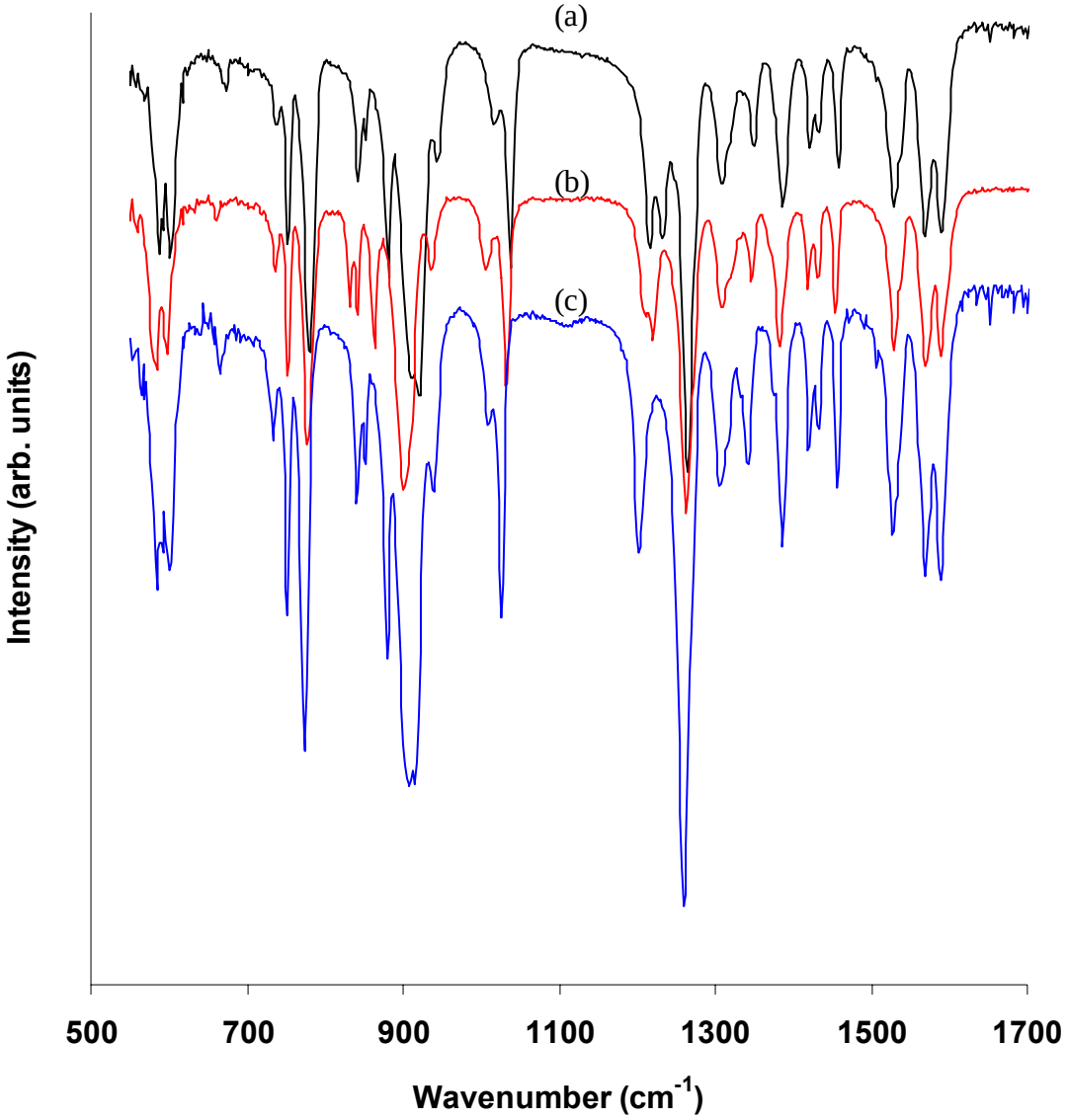

Figure 3.2 Experimental FTIR spectra for RDX and isotopically labeled RDX from 500 to 1600 cm^{-1}; (a) RDX solid (black); (b) $^{13}C_3$-RDX (red); and (c) $^{15}N_3$-RDX (blue).

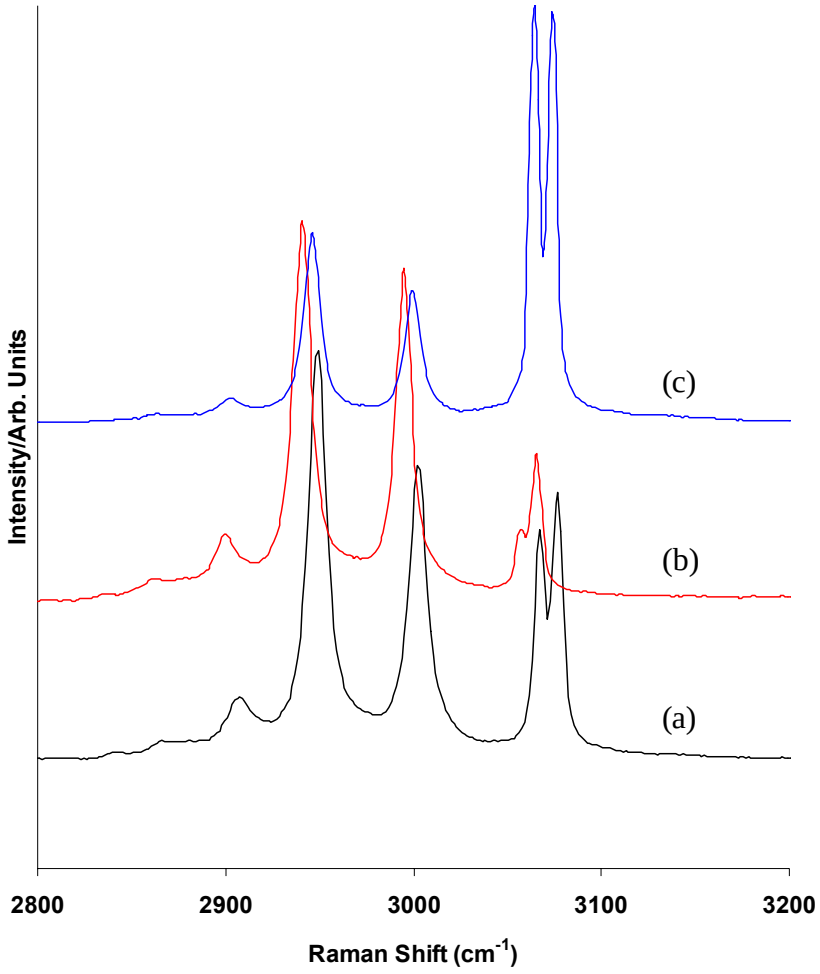

Figure 3.3 Experimental Raman spectra for RDX and isotopically labeled RDX from 2800 to 3200 cm^{-1}. (a) RDX solid (black); (b) $^{13}C_3$-RDX (red); and (c) $^{15}N_3$-RDX (blue).

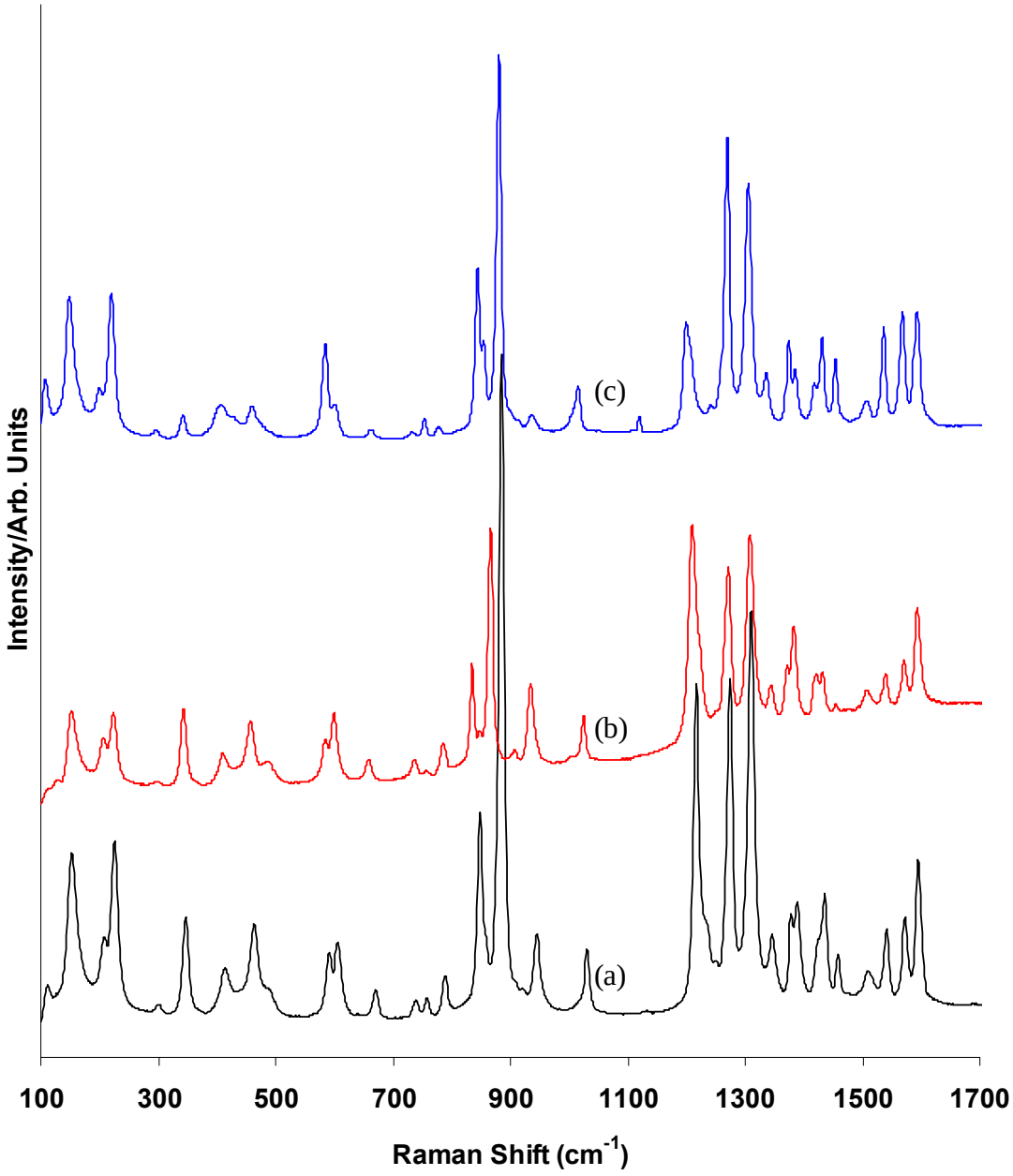

Figure 3.4 Experimental FT-Raman spectra for RDX and isotopically labeled RDX from 100 to 1700 cm^{-1}. (a) RDX solid (black); (b) $^{13}C_3$-RDX (red); and (c) $^{15}N_3$-RDX (blue).

Regarding band intensities, the calculation predicts the observed spectra with sufficient accuracy as a qualitative guide for the vibrational assignment, although there are some problems in a quantitative point of view. Four bands are observed in the region from 2800 to 3200 cm^{-1}. The three bands at 3076, 3067, and 2945 are assigned to CH_2 equatorial asymmetric stretching modes. The band at 2995 cm^{-1} is attributed to asymmetric stretching mode of the CH_2 axial group. The isotopic effect is well observable for the CH_2 stretching modes. The change from ^{12}C to ^{13}C decreased more or less the frequencies in these cases. The asymmetric stretching modes for NO_2 groups are found in the 1520-1600 cm^{-1} region. Of these three signals, two are attributed to axial nitro groups in the triazine ring. In the NO_2 stretching region, the $^{15}N_3$RDX frequency calculation is partially unsuccessful to reproduce the Raman experimental spectrum for this isotopomer. Isotopic mass change has no evident effect on the frequencies for these bands.

The experimental IR and Raman spectra between 1300 and 1460 for α-RDX and its isotopomers show a seven-band pattern. Assignment of the observed vibrational bands is proposed in Table 1. In this sense, it would be important to mention that the vibrational modes in this range seem to reflect the in-plane, $\beta(CH_2)$, and out-of-plane, $\gamma(CH_2)$, methylene bending vibrations. The bending CH_2 vibration, does not shift much in energy for $^{13}C_3$ and $^{15}N_3$, revealing the lack of involvement of the triazine ring in these modes. There are many combinations in the Raman and IR spectra of RDX and its isotopomers below 1300 cm^{-1}.

Several of the bending modes in the spectra of α-RDX were calculated to have small degree of mixing with other vibrations. The symmetric nitro stretch mode mixes with the out-of-plane methylene $\gamma(CH_2)$.Vibrational signals below 1200 cm^{-1} are expected to belong to ring modes and NO_2 bending modes. Vibrations in the region of 800-1200 cm^{-1} are related to ring, N-C-N, C-N-C and nitro deformation, $^{13}C_3$RDX and $^{15}N_3$RDX spectra had small red shifts. The strong Raman peak centered at 885 cm^{-1} is attributed to the symmetric ring-breathing mode. The 1215 cm^{-1} band corresponds to the $\nu(N\text{-}NO_2)$ vibration. The comparative analysis of vibrational modes of RDX and its isotopic analogue shows that patterns and regions of absorption/scattering are very similar. In the case of the C-N stretching the shift depends practically on the participation in the normal mode.

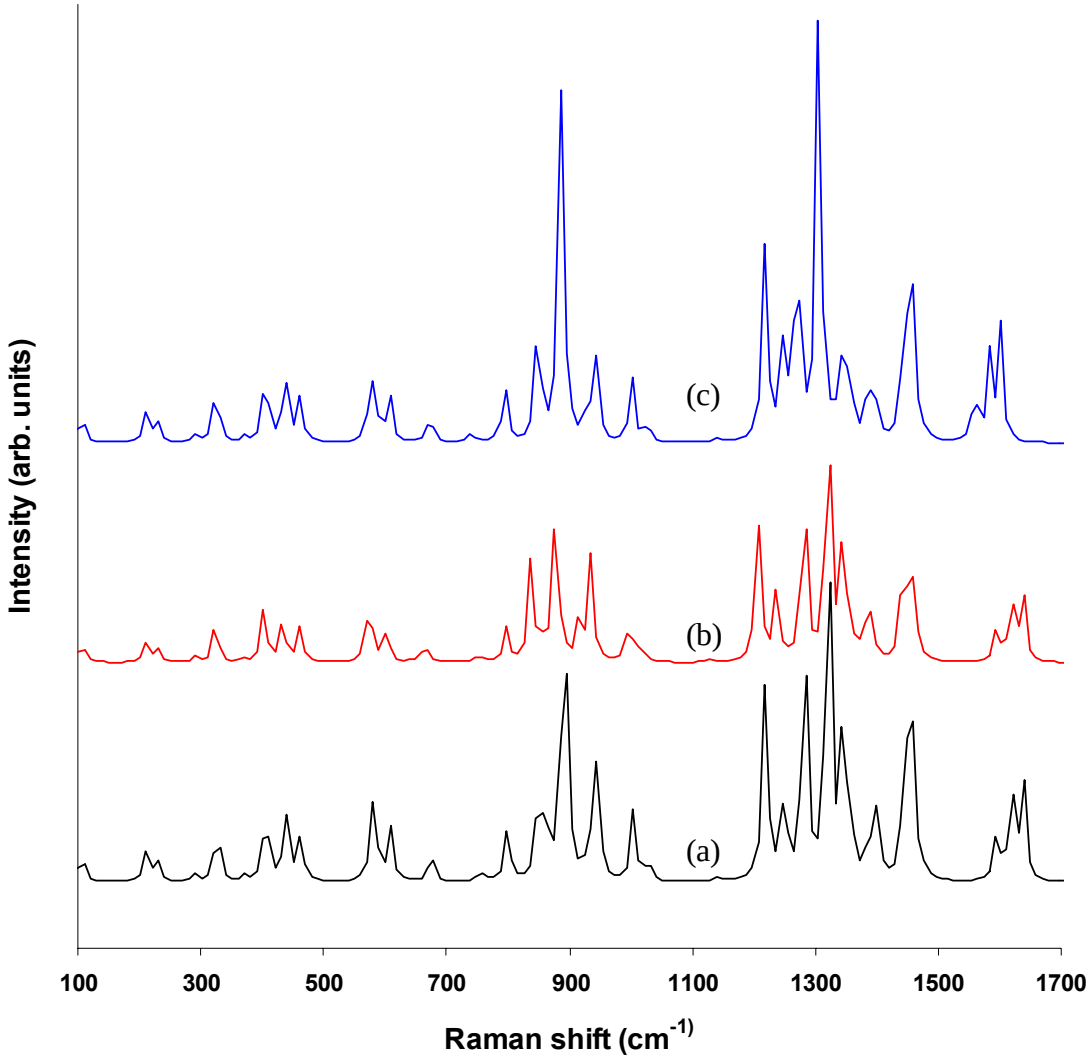

Figure 3.5 Theoretical Raman spectra (B3LYP/6-311+G**) for RDX and isotopically labeled RDX from 100 to 1700 cm^{-1}; (a) RDX normal (black); (b) $^{13}C_3$-RDX (red); and (c) $^{15}N_3$-RDX (blue).

Table 3.1 Observed, calculated and assigned frequencies of fundamental modes for α-RDX, $^{13}C_3$RDX and $^{15}N_3$RDX isotopomers[a]

Mode No.	RDX			^{13}C-RDX			^{15}N-RDX			Assignment[bc]
	IR (cm^{-1})	Raman (cm^{-1})	Calc.[a] (cm^{-1})	IR (cm^{-1})	Raman (cm^{-1})	Calc.[a] (cm^{-1})	IR (cm^{-1})	Raman (cm^{-1})	Calc.[a] (cm^{-1})	
1	3072	3076	3071	3062	3065	3061	3074	3074	3070	$\nu^{as}\ CH_2^{(Eq)}$
2	3064	3067	3065	3054	3057	3059	3064	3064	3069	$\nu^{as}\ CH_2^{(Eq)}$
3	/	3003	2953	/	2995	2950	/	2999	2957	$\nu^{as}\ CH_2^{(Ax)}$
4	/	2949	2894	/	2941	2891	/	2945	2898	$\nu^{as}\ CH_2^{(Eq)}$
5	1589	1595	1636	1589	1594	1637	1589	1592	1601	$\nu^{as}\ NO_2^{(Ax)}$
6	1567	1573	1618	1569	1571	1618	1569	1568	1594	$\nu^{as}\ NO_2^{(Ax)}$
7	1527	1541	1594	1529	1541	1594	1527	1537	1583	$\nu^{as}\ NO_2^{(Eq)}$
8	1457	1459	1472	1454	1453	1468	1456	1453	1471	$\beta CH_2^{(Eq)}$
9	1430	1435	1445	1430	1434	1442	1432	1431	1444	$\beta CH_2^{(Ax)}$
10	1421	/	1399	1419		1391	1419	/	1395	$\gamma\ CH_2^{(Eq)}$
11	1386	1388	1385	1382	1384	1378	1386	1385	1383	$\gamma\ CH_2^{(Ax+Eq)}$
12	/	1377	1354	/	1372	1354		1373	1355	$\gamma\ CH_2^{(Ax)}$
13	1348	1347	1343	1346	1345	1341	1340	1336	1342	$\gamma\ CH_2^{(Eq)}$
14	1307	1310	1319	1309	1309	1320	1305	1304	1304	$\gamma\ CH_2^{(Ax+Eq)}$
15	/	1274	1282	/	1273	1282	1259	1268	1271	$\nu^{s}NO_2^{(Ax)}$+ $\gamma CH_2^{(Ax)}$
16	1265	/	1279	1263	/	1278	/	/	1269	$\nu^{s}NO_2^{(Ax)}$+ $\gamma CH_2^{(Ax)}$
17	1232	/	1248	1220	/	1236	/	/	1246	ν^{s} N-C-N
18	1216	1218	1216	1209	1209	1210	1201	1198	1215	$\nu NNO_2^{(Ax+Eq)}$
19	1037	1032	1027	1031	1025	1015	1025	1014	1026	$\gamma\ CH_2^{(Ax+Eq)}$
20	1016	/	1003	1006	/	996	1008	/	1000	$\nu^{s}NNO_2^{(Ax)}$ + $\gamma CH_2^{(Eq)}$
21	943	946	944	935	936	934	937	/	942	νrg
22	908	/	903	900	/	891	879	880	900	νrg + νN-C
23	881	885	890	863	867	876	850	/	885	Rg breathing $\nu NNO_2^{(Ax+Eq)}$
24	852	849	865	840	/	858	840	842	856	$\delta NO_2^{(Ax)}$+ δC-N-C
25	842	/	850	831	835	837	/	/	845	$\delta NO_2^{(Eq)}$+ δC-N-C
26	779	/	798	777	/	796	773	/	793	δrg
27	752	/	753	752	/	751	752	/	736	$\gamma\ NO_2^{(Eq)}$
28	601	606	608	597	600	602	599	602	606	mix β rg
29	588	591	587	584	585	579	584	586	585	δrg
30	/	463	463	/	457	461	/	/	461	δN-C-N
31	/	348	438	/	344	433	/	/	436	$\beta CH_2^{(Ax+Eq)}$
32	/	226	228	/	224	227	/	221	228	δC-N-C

[a] Calculated with B3LYP/6-3411++G**; scaled according to correlation equation 3.1.

[b] Vibrational modes: ν, stretching; β, bending in plane; γ, bending out-of- plane; rg, ring; δ, deformation; superscript *s*, symmetric; superscript *as*, asymmetric; superscript Ax, axial; superscript Eq, equatorial.

[c] Estimated graphical representation

4 MONITORING α→β PHASE TRANSITION OF RDX WITH FT-RAMAN SPECTROSCOPY

4.1 Introduction

The cyclic nitramine hexahydro-1,3,5-trinitro-*s*-triazine, commonly known as RDX, is an important energetic material for various propellants and explosives formulations. In solid state, RDX exist in four polymorphs: α, β, γ and δ (Dreger and Gupta, 2007). Previous works have established α-phase as the stable form at room temperature, where the six-member ring RDX molecules posses essentially Cs symmetry with two of the NO_2 groups axial and the third equatorial with respect to the triazine ring. This molecular conformation is usually referred as the chair AAE conformer. The thermal solid-solid transition from α-RDX to β-RDX at atmospheric pressure occurs at 204°C. Also, the β-polymorph is obtained either by evaporation of boiling solvent containing RDX (Brill et al., 1983) or by deposition of RDX from solution on a glass substrate (Castro et al., 2004). The molecular conformation of RDX in the β-solid, in solution and in the vapor phase has a molecular symmetry of C_{3v} and two possible structures with this symmetry are possible. One structure has the nitro groups occupying all axial positions (AAA), and the other has the nitro groups occupying all pseudo equatorial positions (EEE). The γ- polymorph was observed under high pressure above 3.8 GPa. The α -γ phase transition is manifested by changes in vibrational spectra patterns and adopts AEE conformation. The γ-RDX phase remains kinetically stable until 18 GPa, approximately. In contrast to the extensive experimental and

theoretical data for α-RDX, there has been limited literature associated with solid β and γ-RDX. Recently we reported the vibrational spectra of solid α-RDX and their fundamental frequencies were assigned using isotopic substitution (Infante-Castillo and Hernández-Rivera, 2007). The structures of the four polymorphs of RDX are shown in Figure 4.1.

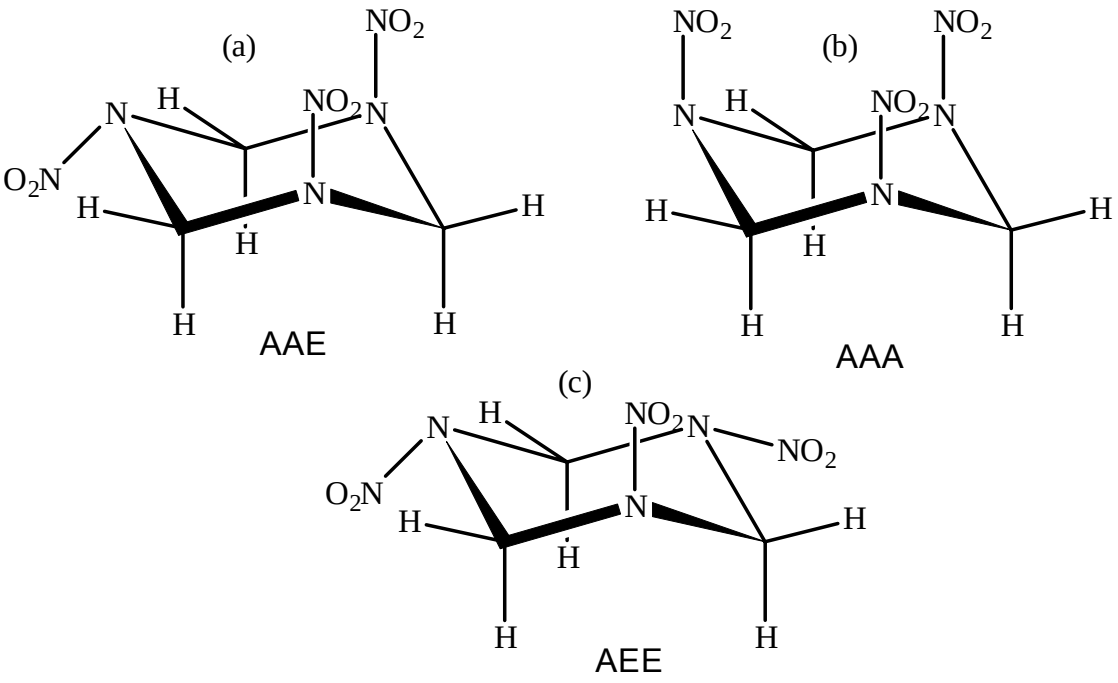

Figure 4.1 Structure of: (a) α-RDX; (b) β-RDX; and (c) γ-RDX

In the present work, IR and Raman spectra of β-RDX were calculated at the DFT/B3LYP level using the 6-311++G(d,p) basis set. The calculated frequencies were compared with experimental data of solid β-RDX and α-RDX. Assignments of the vibrational modes for β-RDX are made through comparison between experimental and density functional calculation results. Using Raman

spectroscopy, we have observed the solid-solid phase transition of RDX in real time. By heating at slow rates and following the spectral details, crystal transformation occurring near the melting point can be seen. The results from these experiments show that once the β-RDX is formed, no reversible change in the symmetry is observed and the Raman spectra differences in both conformers are evident.

4.2 Results

Absolute, relative and zero-point energies for AAA and AAE conformers of RDX, obtained by B3LYP/6-311G++**, are shown in Table 4.1. The results of the calculations indicate that the AAA conformer is only slightly lower in energy than the AAE conformer (by 0.02 kcal/mol). Within the level accuracy for the calculations, the AAE and AAA conformers are identical in their stability. Previous theoretical calculations had the energy ordering reversed for the AAE and AAA conformers. In these studies, the AAE was more stable by 0.64, 0.52 and 0.19 kcal/mol using 6-311+G**, 6-311G** and 6-31G * respectively.

Having obtained the room temperature spectra of the α-RDX, a great deal of effort was directed at the use of Raman spectroscopy to map the solid-solid temperature-induced transition of RDX. Figure 4.2 shows the typical spectral changes which occur upon slow heating of RDX and then cooling to room temperature. The α-polymorph was stable until 203°C.

Table 4.1 Absolute and relative energies of RDX conformers

Conformer	Absolute Energy (hartrees)	Zero-point Energy (kcal/mol)	Relative Energy (kcal/mol)
AAE[a]	-897.65548	99.55	0.00
AAA[a]	-897.65465	99.41	0.52
AAE[b]	-897.679561	89.11	0.00
AAA[b]	-897.678331	88.98	0.64
AAE[c]	-897.409356	83.57	0.00
AAA[c]	-897.408901	86.47	0.19
AAE[d]	-897.684630	89.11	0.02
AAA[d]	-897.674094	88.92	0.00

a. Harris and Lammertsma, 1997
b. Rice and Chabalowski, 1997
c. Rice and Vladimiroff, 2002
d. this work

Above 204°C various changes in the Raman spectra confirm the occurrence of the $\alpha \rightarrow \beta$ phase transition. Temperature-induced effects on the C-H stretching modes in Raman spectra are shown in Fig. 4.3.

Calculated spectra based upon B3LYP/6-311++G** Raman frequencies and intensities for the three conformers are compared against experimental α and β-RDX spectra in Figure 4.4. Based on the comparison between the calculated and experimental spectra, it is clear that the calculated spectrum for the AAA conformer has several features that are similar to experimental β-solid phase spectrum. The theoretical Raman spectrum for EEE conformer shows a band pattern in much poorer agreement with the experimental β-RDX spectrum. The assignments of normal vibrations of RDX and α/β conformers are presented in Table 4.2, listing the experimental and the calculated scaled frequencies.

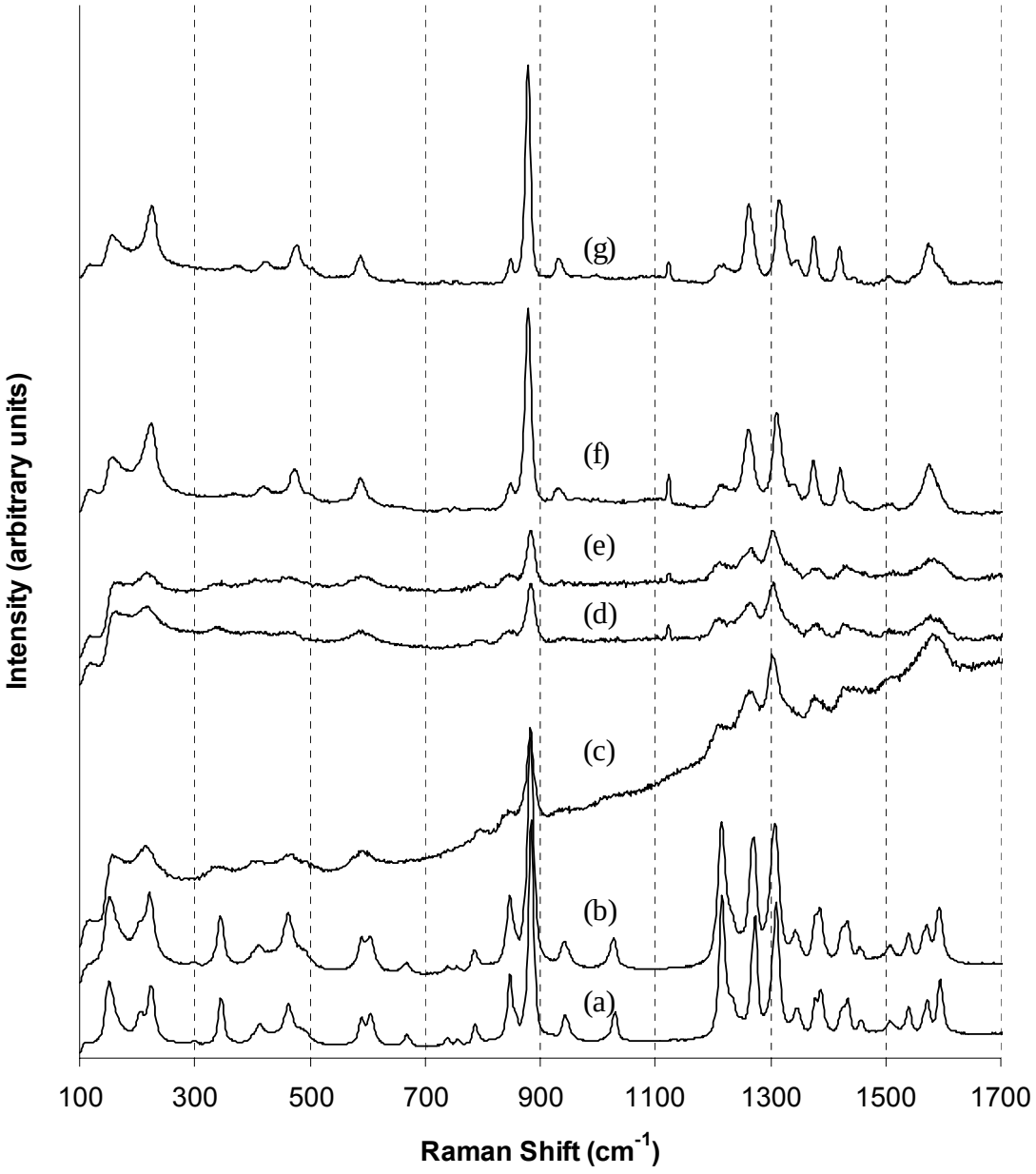

Figure 4.2 Raman spectral changes upon slow heating α-RDX to 204°C and then cooling to room temperature; a α→β RDX transition occurs. Heating: (a) 25°C; (b) 150°C; (c) 202°C; (d) 204°C. Cooling: (e) 202°C; (f) 150°C; (g) 25°C.

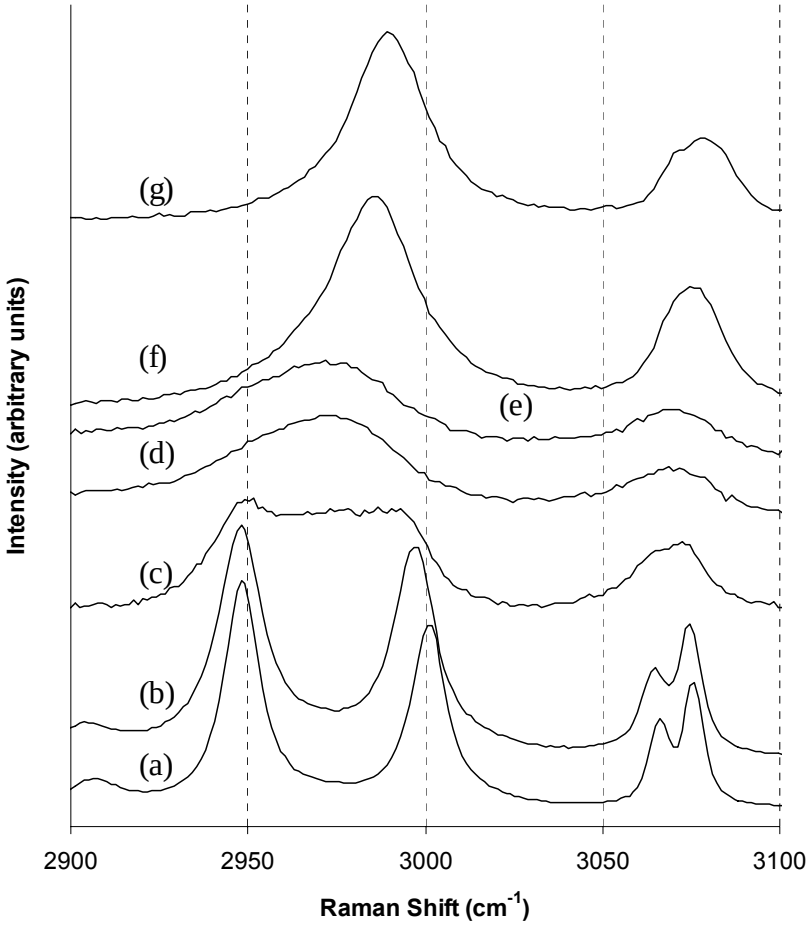

Figure 4.3 Effect of temperature on Raman modes in the frequency range 2900-3200 cm^{-1}. Heating: (a) 25°C; (b) 150°C; (c) 202°C; (d) 204°C. Cooling: (e) 202°C; (f) 150°C; (g) 25°C.

For a better comparison of the predicted harmonic wavenumbers with the recorded wavenumbers of the fundamental modes, we scaled the DFT calculated vibrational frequencies using wavenumber-linear scaling method (Hiroshi and Akito, 2000). The scaled calculated frequencies of the molecules investigated are very close to the corresponding experimental values.

4.3 Discussion

Various changes in the spectra at 204°C confirm the occurrence of the $\alpha \rightarrow \beta$ phase transition. The decrease in the number of peaks in the Raman spectra is in general an indicative of the increase in molecular symmetry. The α-RDX and β-RDX phases have 37 and 24 active Raman signals, respectively. The most obvious changes in the Raman spectrum are observed in the C-H stretching region. The Raman spectrum at 25 and 150°C shows bands characteristic of solid α-RDX. Solid α-RDX has close to C_s symmetry and occupies a C_1 site. The 57 fundamental vibration modes are active in both IR and Raman. Four bands are observed in the region from 2800 to 3200 cm^{-1}. The three bands at 3076, 3067, and 2945 are assigned to CH_2 equatorial asymmetric stretching modes. The band at 2995 cm^{-1} is attributed to asymmetric stretching mode of the CH_2 axial group. The assignments for the experimental Raman and IR absorption frequencies for α and β-RDX are listed in Table 4.2. The increase in symmetry from Cs to C3v is consistent with the decrease in the numbers of modes in the spectrum of β-RDX. The reported experimental Raman frequencies

for the β-RDX are comparable with the ones obtained theoretically for AAA conformer. The doublet at 3076 and 3067 cm^{-1} coalesces into a single band at 3077 cm^{-1} in β-RDX. The single band at 2987 cm^{-1} in the spectrum of β-RDX corresponds to convergence of the bands at 2995 and 2945 cm^{-1} in the spectrum of α-polymorph. Figure 4.2 shows the effect of temperature on Raman modes in the region from 2800 cm-1 to 3200 cm^{-1} for both phases β and α-RDX. Three Raman bands found in the 1520-1600 cm^{-1} region in the spectrum of α-RDX are readily assigned to asymmetric stretching modes for NO_2 groups. Of these three signals, two are attributed to axial nitro groups in the triazine ring. In contrast, only one band at 1527 cm^{-1} can be observed for β-RDX. The existence of a broad band with a shoulder in the β phase reaffirms that the NO_2 groups in the β phase have approximately the same chemical environmental with all the NO_2 groups in axial position. It is clear that the CH and NO_2 stretching regions in the Raman spectra are really sensitive to polymorphic changes in the RDX molecule. The convergence of the Raman modes under high temperature condition serves as a clear marker of the phase transitions.

The experimental Raman spectrum between 1100 and 1460 for α-RDX show a seven-band pattern, while in β-RDX only four modes were observed. Assignment of the observed vibrational bands is proposed in Table 4.2. In this sense, it would be important to mention that the vibrational modes in this range seem to reflect the in-plane, $\beta(CH_2)$, and out-of-plane, $\gamma(CH_2)$, methylene bending vibrations and the stretching N-NO_2. The calculated modes for AAA assigned in

the previous region coincide with the experimental β-phase. The single bands at 1418 and 1374 cm^{-1} in the spectrum of β-RDX corresponds to convergence of the bands at 1436/1460 and 1380/1390 cm^{-1} respectively in the spectrum of α-polymorph. These modes shift to lower frequencies. The band at 1314 cm^{-1} in the β phase decreases frequency to 1310 cm^{-1} in the α phase. The band ca. 1273 cm^{-1} in the α phase moves to 1260 cm^{-1} in the β phase. At 1214 cm^{-1} a strong band was observed for α phase. This mode corresponds to γ CH2 equatorial and does not appear in β phase spectrum. An intense band appears at 884 cm^{-1} in the α phase. When the change of phase occurs from the α to β phase, the band moves to 878 cm^{-1}. In both phases this band has the most intense absorption. The band found at 587 cm^{-1} in the β phase corresponding to a ring rotation plus a C-N stretching mode is split into a doublet at 592 cm^{-1} and 907 cm^{-1} in the α phase. These vibrational modes were assigned to a ring bending and a ring rocking respectively

A group of weak bands at 1031, 789, 670 and 346 cm^{-1} in the α phase are not detected in the Raman spectrum for the β phase. On the other hand, the bands at 413 cm^{-1} and 465 cm^{-1} in the α phase are assigned to ring breathing modes (only carbons atoms) and ring breathing respectively, move to 420 cm^{-1} and 476 cm^{-1} in the β phase. These bands at 413 cm^{-1} and 465 cm^{-1} in the α phase were assigned to a ring bending and a ring bending plus an N-N stretching (axial) vibration respectively. The band at 225 cm^{-1} in α and β phases was assigned to a ring rotation plus an NO_2 rocking motion.

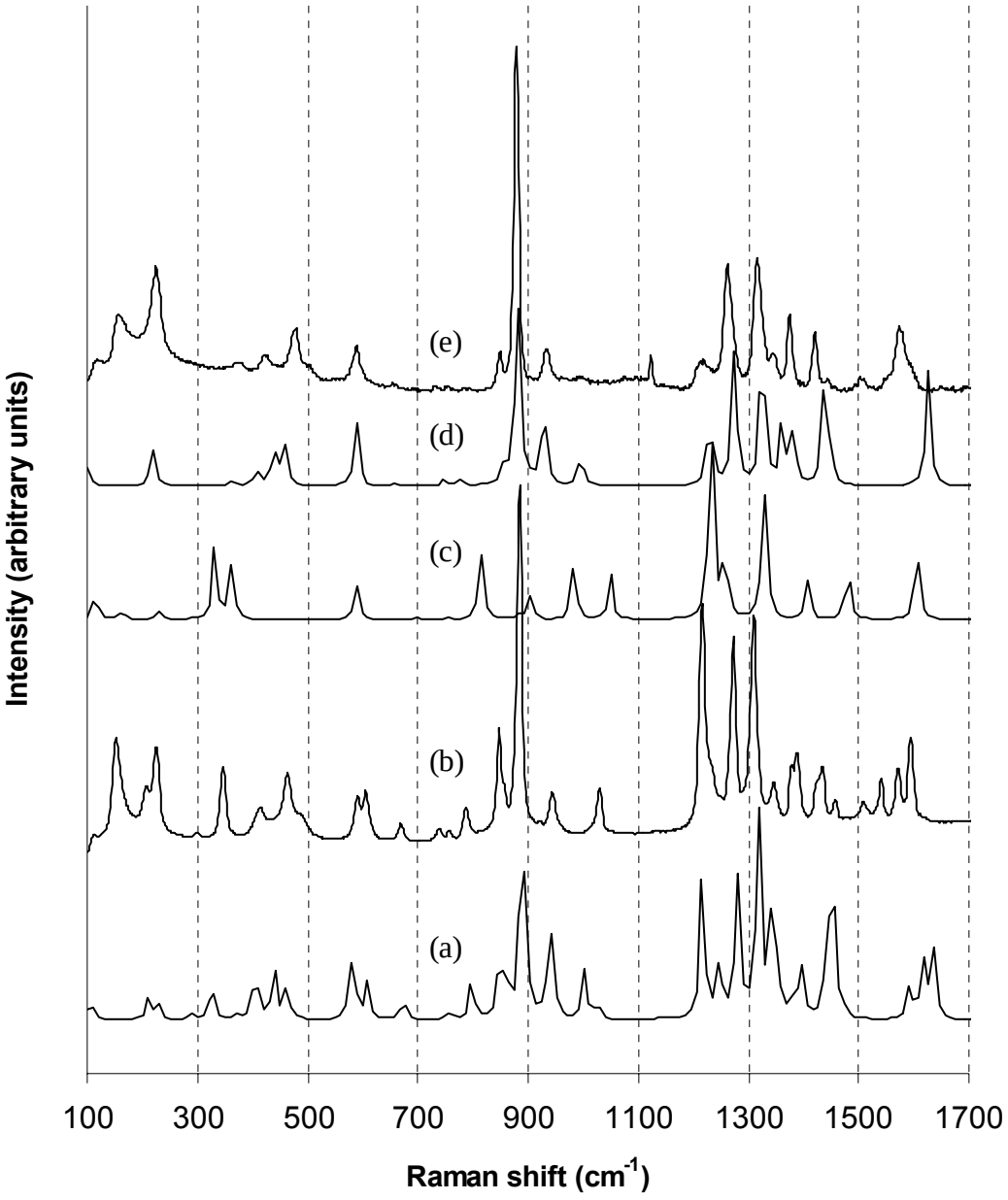

Figure 4.4 Theoretical and experimental FT-Raman spectra for RDX and conformers from 100 to 1700 cm^{-1} using B3LYP/6-311++G**: (a) calculated AAE RDX conformer, (b) experimental α-RDX, (c) calculated EEE-RDX conformer, (d) calculated AAA-RDX conformer and (e) experimental β-RDX.

Table 4.2 Observed, calculated and assigned frequencies of fundamental modes for α and β-RDX

Mode No.	α-RDX (AAE)[a]			β-RDX		(AAA)	(EEE)	
	IR (cm^{-1})	Raman (cm^{-1})	Calc.[b] (cm^{-1})	IR[e] (cm^{-1})	Raman (cm^{-1})	Calc.[b] (cm^{-1})	Calc.[b] (cm^{-1})	Assignment[cd]
1	3072	3076	3071	3075	3073	3051	3060	ν^{as} $CH_2^{(Eq)}$
2	3064	3067	3065	3067	/	/	/	ν^{as} $CH_2^{(Eq)}$
3	/	3003	2953	3005	2987	2943	/	ν^{as} $CH_2^{(Ax)}$
4	/	2949	2894	/	/	/	2842	ν^{as} $CH_2^{(Eq)}$
5	1589	1595	1636	1588	/	/	/	ν^{as} $NO_2^{(Ax)}$
6	1567	1573	1618	/	1572	1627	/	ν^{as} $NO_2^{(Ax)}$
7	1527	1541	1594	/	/	/	1608	ν^{as} $NO_2^{(Eq)}$
8	1457	1459	1472	1458	/	/	1484	βCH_2
9	1430	1435	1445	/	/	/	/	βCH_2
10	1421	/	1399	1419	1418	1435	1407	βCH_2
11	1386	1388	1385	1383	/	1378	/	γ CH_2
12	/	1377	1354	/	1374	/	/	γ CH_2
13	1348	1347	1343	/	1342	1359		γ CH_2
14	1307	1310	1319	1313	1314	1320	1330	$\nu N\text{-}NO_2+\gamma CH_2$
15	/	1274	1282	/	/	/	/	$\nu N\text{-}NO_2$
16	1265	/	1279	1261	1261	1272	1234	$\nu N\text{-}NO_2$
17	1232	/	1248	/	/	1234	/	ν^{s} N-C-N
18	1216	1218	1216	1218	/	1224	/	ν N-C
19	1037	1032	1027	/	/	/	1049	γ CH_2
20	1016	/	1003	1018	/	991	981	$\nu^{s}NNO_2+\gamma CH_2$
21	943	946	944	931	931	932	/	νrg
22	908	/	903	904	/	/	/	νrg
23	881	885	890	877	878	883	903	rg breathing
24	852	849	865	/	/	/	/	$\delta NO_2+\delta$C-N-C
25	842	/	850	845	846	/	/	$\delta NO_2+\delta$C-N-C
26	779	789	798	774	/	/	815	δrg (N-C-N)
27	752	/	753	/	/	/	/	γ NO_2
28	/	670	677		/	/	/	δ rg
28	601	606	608	/	/	/	/	mix β rg
29	588	591	579	/	587	588	588	$\beta CH_2+\beta NO_2$
30	/	463	463	/	476	460	/	δrg (N-C-N)
31	/	413	410	/	420	440	360	βCH_2
32	/	348	330	/	/	/	330	βCH_2
33	/	226	230	/	225	220	/	τ $NO_2+\delta$ rg

[a] (Infante and Hernandez, 2004) [b] Calculated with B3LYP/6-3411++G**; scaled according to equation 3.1 (Yoshida, 2000). [c]Vibrational modes: ν, stretching; β, in plane bending; γ, out-of-plane bending; rg, ring; δ, deformation; τ , torsion; *s*, symmetric; *as*, asymmetric; Ax, axial; Eq, equatorial.[d] Estimated graphical representation. [e] (Karpowicz and Brill, 1984)

5 ^{13}C AND ^{15}N NMR CHEMICAL SHIFTS CALCULATIONS ON NITRAMINE SYSTEMS: A COMPARISON OF METHODS AND BASIS SETS

5.1 Introduction

It is well known that nuclear magnetic resonance (NMR) is one of the most powerful and extensively used experimental methods to probe the electronic and molecular structures of a wide range of compounds. A significant part of the NMR spectral information is the chemical shifts, which are used in structural assignments. Liquid solution NMR is one of the techniques that have been used to study energetic materials. Relationships between liquid-state isotropic chemical shift and explosive characteristics have been illustrated by Zeman and colleagues. In this sense, theoretical NMR chemical shifts calculations have been proved to be a useful tool to interpret experimental data. The calculation of nuclear magnetic resonance (NMR) parameters is an important aspect of theoretical chemistry. The measured NMR spectra in combination with theoretical calculation lead to nearly unequivocal structural assignments of the system under study (Infante et al., 2008). It is known that large basis set are required to calculate accurate magnetic shielding values and also that a correction for electron correlation is desirable. Density functional theory (DFT) has emerged as an approximate but computationally inexpensive method of treating electron correlation that gives performance comparable to a second order Møller-Plesset theory (MP2) and has already yielded promising results for the calculation of NMR shieldings (Gauss, J. and Stanton, 2002). The root mean square (RMS)

error achieved at B3LYP/6-311+G(2d,p) level for ^{13}C chemical shifts was 4.2 ppm (Cheeseman J. et al., 1996)

The relationship between detonation characteristics and ^{15}N NMR chemical shifts of nitramines was reported by Zeman (Zeman, 1999). The electron configuration and steric conditions with the reaction centre of the molecule can be represented by NMR chemical shifts of the key atoms of the centre. The shifts of these atoms should correlate with characteristics of individual energetic materials. That means that the centers of initiation (hot spots) reactivity in molecules of nitramines can be advantageously determined by means of ^{15}NMR spectroscopy (Zeman S, 2006).

A number of computational methods have been developed for the calculation of nuclear magnetic shielding tensors. It is generally accepted that accurate prediction of these properties within the finite basis approximation requires gauge-invariant procedures (Facceli, 2004). This contribution will focus on predicting NMR shielding tensors at DFT/B3LYP level of theory with two different models, gauge-including atomic orbital (GIAO) (Ditchfield, 1974) and continuous set of gauge transformations (CSGT) (Keith and Bader, 1993) and two different basis set, 6-311+G(2d,p) and cc-pvtz (Dunning and Woon, 1995). The solvent effect on the theoretical NMR parameters was included using Integral Equation Formulation-Polarizable Continuum Model (IEF-PC). The consistency and efficiency of the considered combinations of models and basis set on NMR calculations were thoroughly checked by the analysis of statistical

parameters concerning computed and experimental ^{13}C NMR/^{15}N NMR chemical shifts values.

The tested nitramines were four acyclic compounds: (1) 1-nitro-1-azaethane (MNA); (2) N,N-dimethylnitramine (DMNA); (3) 1,1-dinitro-1-1aza-ethane (MDN); (4) N,N-diethylnitroamine (DENA) and six cyclic compounds: (5) 1,3-dinitro-1,3-diazacyclobutane (TETRAGEN); (6) 1,1,3-trinitroazetidine (TNAZ); (7) 1,3-dinitro-1,3-diazacyclopentane (CPX); (8) N-nitropiperidine (NP);(9) 1,4-dinitro-1,4-diazacyclo-hexane (DNDC) and (10) Hexahydro-1,3,5-trinitro-s-triazine (RDX) (see Figure 5.1). Molecules of nitromethane and tetramethylsilane (TMS) were also included as a reference compounds.

In addition, we also report the ^{15}N chemical shift tensors of α-RDX and discuss the theoretical model necessary to accurately calculate these values. The β-polymorph is obtained in solution NMR studies. The multiple nitrogen sites and structural sensitivity of ^{15}N chemical shifts provide an opportunity to use ^{15}N solid-state NMR spectroscopy to study the subtle differences present in the RDX polymorphs.

Based on the present study, we suggest that, among the methods and basis sets taken into consideration, the best prediction of the ^{13}C and ^{15}N values is obtained at the CSGT model using 6-311+G(2d,p) basis set . Theoretical NMR chemical shifts calculations have proved to be a useful tool to interpret experimental data. The measured NMR spectra in combination with theoretical calculation lead to nearly unequivocal structural assignments of the system under this study.

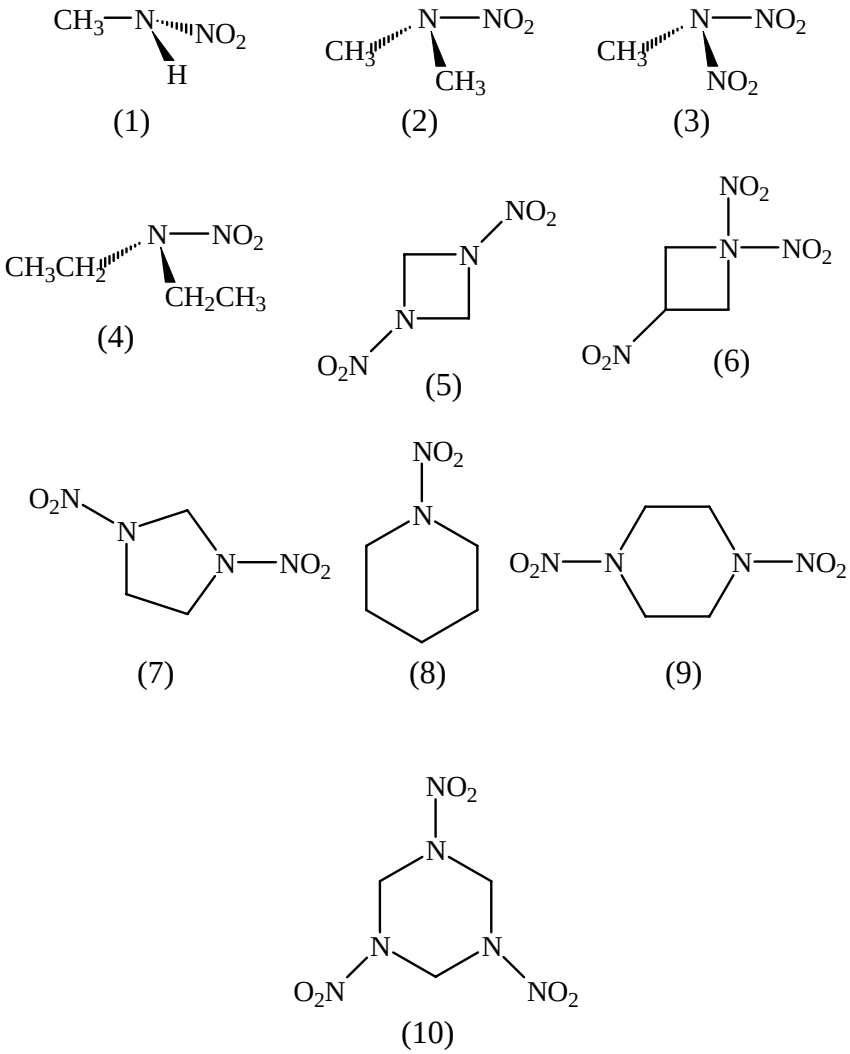

Figure 5.1 The structures of the investigated compounds. (1) 1-nitro-1-azaethane (MNA); (2) N,N-dimethylnitramine (DMNA); (3) 1,1-dinitro-1-1aza-ethane (MDN); (4) N,N-diethylnitroamine (DENA); (5) 1,3-dinitro-1,3-diazacyclobutane (TETRAGEN); (6) 1,1,3-trinitroazetidine (TNAZ):(7) 1,3-dinitro-1,3-diazacyclopentane (CPX); (8) N-nitropiperidine (NP);(9) 1,4-dinitro-1,4-diazacyclohexane (DNDC) and (10) Hexahydro-1,3,5-trinitro-s-triazine (RDX)

In this sense, theoretical calculations of the chemical shifts may be used as an aid for the assignment of the experimentally determined shifts and for the study of the conformational behavior of the molecules. The values of the chemical shielding constants strongly depend on the geometry of the molecule. Chemical shielding constants are frequently calculated by the density functional theory (DFT) approach because it provides better results than conventional SCF-based methods with comparable computational effort.

5.2 Results

In Tables 5.1 and 5.2 the calculated NMR chemical shifts in solution is compared with the experimental data for ten nitramines. The DFT method with the B3LYP and 6-311G(d,p) hybrid functional was used to generate the optimized structure of the studied compounds. The ^{13}C and ^{15}N chemical shielding calculations were converted into the predicted chemical shifts using tetramethylsilane and nitromethane values calculated at the same level of the theory. The NMR experiment was measured in acetone and dimethylsulfoxide solutions. The predicted chemical shift values of DFT method are very suitable to the NMR experimental values. The theoretical calculations of ^{15}N and ^{13}C NMR chemical shifts for acyclic nitramines (Table 5.1) and cyclic nitramines (Table 5.2) were performed with GIAO and CSGT model, through B3LYP level of theory applying two different basis sets. Based on the ^{13}C and ^{15}N chemical shifts, data presented in Table 5.1 and 5.2 an the fits (Figure 5.2) one can deduce that the select DFT method, combined with appropriate model and basis set, represents

a good compromise between accuracy and computational time, and yielded carbon and nitrogen chemical shifts in a agreement with experimental values. Results of linear regression fits between experimental and calculated chemical shifts (^{13}C) performed for the ten nitramines tested are summarized in Table 5.3. The regression coefficients (R^2) between calculated and experimental chemical shifts range from a high of 0.991for ^{13}C in CSGT/cc-pvtz model to a low 0.979 in GIAO/cc-pvtz model. The ^{15}N amine chemical shifts in acyclic nitramines show a very good correlation coefficient, R^2= 0.997 ± 0.001 using CSGT model in both basis set (6-311+G(2d,p) and cc-pVTZ. Most of the experimental chemical shifts were smaller than the calculated values. The largest deviations from experimental values were observed in the ^{15}N (amine) calculated chemical shifts. Figure 5.3 shows the effects of the basis sets in the GIAO and CSGT calculations when the geometry optimizations of the structures utilized as inputs in the GIAO and CSGT calculations were performed at DFT theory. The solid-state CP/MAS ^{15}N NMR spectrum of RDX is shown in Figure 5.4.

5.2 Discussion

The CSGT/6-311+G(2d,p) approach has proved to be the most efficient in predicting the ^{13}C chemical shifts of the compounds taken in consideration, displaying both the lowest mean absolute error (MAE) parameters and the highest linear correlation coefficients (R^2). This is illustrated in Figure 5.3 and is supported by the results in Tables 5.3 and 5.4.

The presence of anomalous trends in reproducing the experimental chemical shifts determined by each combination of models of NMR parameters calculations and basis sets could be outlined by the consideration of Table 5.4 and by visual analysis on Figure 5.3. For the GIAO and CSGT calculations, it is interesting that a general overestimation of ^{15}N-(amine/nitro) chemical shifts occurs using the 6-311+G (2d, p) and cc-pvtz basis sets respectively. The corresponding MEA values are 11.52/8.25 and 9.80/846. In contrast best result were obtained using 6-311+G(2d,p) basis set together with CSGT model. The R^2 values reported in Table 5.3 suggest that the improvement of the ^{13}C-NMR results involved CSGT model and cc-pVTZ basis set. However, the use of 6-311+G(2d,p) basis set in the ^{13}C CSGT calculations provide better results according to the lowest MEA value.

The results from Table 5.3 and 5.4 shows for GIAO model slight discrepancies between theoretical and experimental data. This behavior could be attributed to some limitation of the GIAO model in describing the effect of the strong electron-withdrawing group (NO_2) in the NMR shielding tensor. To evaluate this hypothesis, the GIAO model was replaced by CSGT to predict the NMR shielding tensors for nitramines 1-10, using 6-311+G (2d, p) and cc-pVTZ basis sets. The CSGT model at B3LYP/6-311+G(2d,p) level, leads to the best agreement between theoretical and experimental data for the ten studied nitramines (Tables 5.1and 5.2).

Table 5.1 ^{13}C and ^{15}N experimental and theoretical chemical shifts for acyclic nitramines at different models and basis set.

Comp.	Experimental		GIAO				CSGT			
			6-311+(2d,p)		cc-PVTZ		6-311+(2d,p)		cc-PVTZ	
	$\delta^{13}C$	$\delta^{15}N$(amine) $\delta^{15}N$(nitro)	$\delta^{13}C$	$\delta^{15}N$(amine) $\delta^{15}N$(nitro)	$\delta^{13}C$	$\delta^{15}N$(amine) $\delta^{15}N$(nitro)	$\delta^{13}C$	$\delta^{15}N$(amine) $\delta^{15}N$(nitro)	$\delta^{13}C$	$\delta^{15}N$(amine) $\delta^{15}N$(nitro)
1	32.40	-220.2 -22.2	35.61	-220.42 -29.53	35.30	-222.09 -28.40	35.34	-222.94 -29.44	35.35	-222.97 -30.17
2	40.00	-215.6 -23.6	40.91	-227.70 -35.41	45.51	-207.34 -18.24	41.70	-213.40 -28.8	41.71	-215.3 -30.34
3	41.50	-89.7 -38.8	43.1	-74.2 -42.35	45.6	-94.31 -57.54	42.2	-81.3 -42.1	43.91	-104 -66.94
4	46.40 11.80	-192.6 -27.6	49.60 12.10	-196.00 -40.01	49.80 12.60	-198.00 -38.00	50.00 12.20	-197.46 -39.54	50.05 12.62	-201 -39.58

Table 5.2 ^{13}C and ^{15}N experimental and theoretical chemical shifts for cyclic nitramines at different models and basis set

Comp.	Experimental		GIAO				CSGT			
			6-311+(2d,p)		cc-PVTZ		6-311+(2d,p)		cc-PVTZ	
	$\delta^{13}C$	$\delta^{15}N$(amine) $\delta^{15}N$(nitro)	$\delta^{13}C$	$\delta^{15}N$(amine) $\delta^{15}N$(nitro)	$\delta^{13}C$	$\delta^{15}N$(amine) $\delta^{15}N$(nitro)	$\delta^{13}C$	$\delta^{15}N$(amine) $\delta^{15}N$(nitro)	$\delta^{13}C$	$\delta^{15}N$(amine) $\delta^{15}N$(nitro)
5	/	-203.62 -27.83	86.64	-226.35 -27.84	86.48	-226.88 -26.42	86.08	-226.40 -26.90	85.95	-229.21 -29.24
6	65.0 105.0	-212	70.73 116.76	-231.90 16.94 28.07	70.55 116.46	-232.67 14.52 26.43	70.11 114.46	-232.41 16.42 27.57	70.24 114.93	-234.16 15.26 28.33
7		-209.01 -31.21	70.86 51.82	-196.09 -35.98	70.95 51.94	-197.02 -34.54	70.20 51.21	-197.52 -35.58	71.11 5205	-200.11 -36.54
8	49.3 25.2 23.8	-196.0 -22.0	47.31 25.24 21.91	-220.35 -40.29	48.59 24.97 21.84	-205.53 -33.97	48.46 24.67 21.75	-203.37 -35.62	48.03 26.53 23.56	-221.33 -40.02
9		-205.49 -26.26	50.69	-200.37 -32.50	50.81	-202.24 -31.77	50.3	-201.82 -32.15	51.14	-203.71 -33.13
10 β-RDX	60.80	-199.10 -34.7	AAA 59.96 EEE 64.49 AAE	AAA -195.17 -44.51 EEE -207.75 -47.61 AAE	AAA 60.16 EEE 65.02 AAE	AAA -195.27 -42.52 EEE -209.33 -45.27 AAE	AAA 59.51 EEE 64.10 AAE	AAA -196.71 -43.67 EEE -209.7 -47.25 AAE	AAA 60.37 EEE 65.14 AAE	AAA -198.37 -44.42 EEE -211.55 -47.3 AAE
α-RDX	61.5	-187.5/-175.4	61.80	-202.1/-193.0 -38.2/-35.8	63.48	-206.7/-195.1 -40.1/-41.0	61.6	-206.4/-196.3 -41.4/-40.9	62.63	-207.6/-196.4 -42.0/-41.3

An important point that should be mentioned is that while the cc-pVTZ basis set gives 534 basis functions for RDX, the 6-311+G(2d,p) gives 441 basis functions which leads to a shorter computational time with the same accuracy level for ^{13}C and ^{15}N NMR chemical shifts.

Different resonances present in the solid-state CP/MAS ^{15}N NMR spectrum suggest the structural sensitivity of ^{15}N chemical shifts. The solid-state CP/MAS ^{15}N NMR spectrum of the solid RDX is compared to the solution spectrum. The solid-phase ^{15}N NMR spectrum of the RDX provides additional resolution over the liquid solution-state spectrum. The two resonances observed in the ^{15}N NMR CP/MAS spectrum (Figure 5.4) from 170 to 190 of RDX suggest that non-equivalent magnetic environment. The relative sizes of the peaks are related, in part, to the number of each type of nitrogen atom present in the molecule. Notice in Figure 5.4 that the peak at 187.5 ppm is much larger than the 175.4 ppm peak. This peak is generated by the two nitrogen atoms with the NO_2 groups in axial position. The ^{15}N NMR spectrum of the solid RDX is significantly different from that in solution. Figure 5.4 shows the amine nitrogen region of the CP/MAS spectrum of RDX.

In a solution ^{15}N NMR spectrum only one amine signal was found while in the solid state there are two. The difference arises because in solution, the molecular symmetry of RDX is C_{3V}, whereas, in the solid, the molecules occupy sites of Cs symmetry and the amine-nitrogen atoms are different. The increase in symmetry from C_s to C_{3V} is consistent with the decrease in the resonance signals in the solution spectrum of RDX.

Table 5.3 Slope (a), intercept (b) and linear correlation coefficient (R^2) found for the different combination of model and basis set for ^{13}C and ^{15}N NMR calculations

Straight-line	a	b	R^2
^{13}C-GIAO/6-311+G(2D,P)	0.97 ± 0.04	0.29 ± 1.67	0.987
^{13}C-GIAO/CC-PVTZ	0.95 ± 0.04	0.20 ± 2.16	0.979
^{13}C-CSGT/6-311+G(2D,P)	0.97 ± 0.04	0.33 ± 1.64	0.987
^{13}C- CSGT / CC-PVTZ	0.99 ± 0.03	-1.14 ± 1.47	0.991
^{15}N-GIAO/6-311+G(2D,P)[a]	0.85 ± 0.04	-26.81 ± 8.37	0.995
^{15}N-GIAO/CC-PVTZ[a]	1.04 ± 0.07	8.80 ± 13.08	0.992
^{15}N-CSGT/6-311+G(2D,P)[a]	0.93 ± 0.04	-13.87 ± 6.80	0.997
^{15}N-CSGT / CC-PVTZ[a]	1.10 ± 0.04	25.50 ± 7.28	0.998

[a] acyclic nitramines

Table 5.4 Mean absolute error (MAE) for the different combination of model and basis set for ^{13}C and ^{15}N NMR calculations

Mean Absolute Error (MAE)			
Model/Basis set	^{13}CNMR	^{15}N(Amine)	^{15}N(Nitro)
GIAO/6-311+G(2d,p)	1.57	11.52	8.25
GIAO/CC-PVTZ	2.22	8.00	7.86
CSGT/6-311+G(2d,p)	1.52	7.33	6.83
CSGT/CC-PVTZ	1.57	9.80	8.46

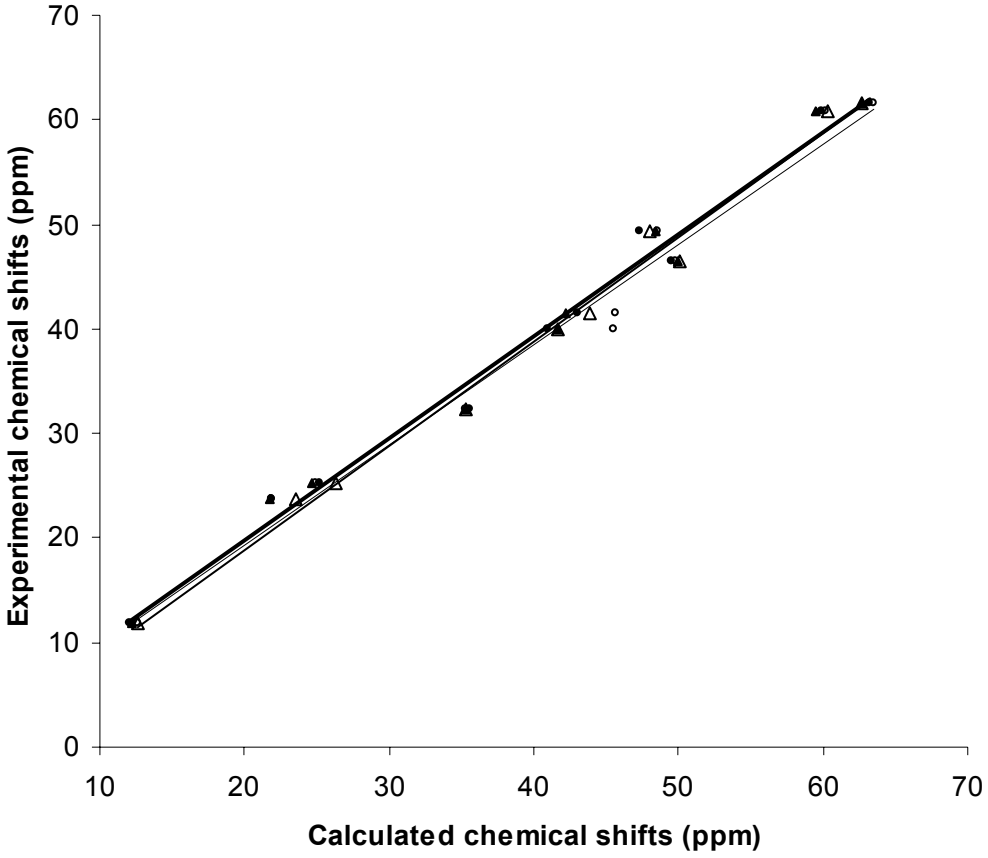

Figure 5.2 The linear regression between experimental and theoretical DFT predicted ^{13}C NMR chemical shifts for cyclic and acyclic nitramines using different models and basis set; ○ GIAO/6-311+G(2D,P), ● GIAO/cc-pVTZ, ▲ CSGT/6-311+G(2D,P), ∆ CSGT/ cc-pVTZ.

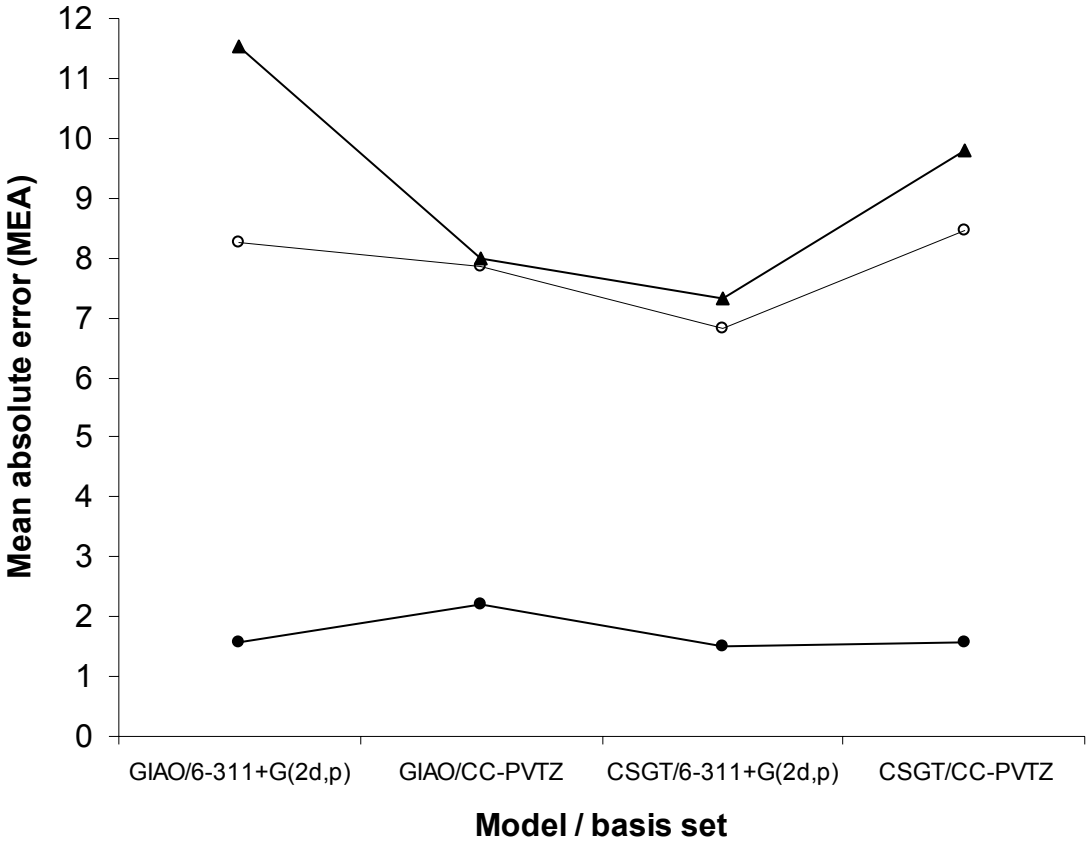

Figure 5.3 Mean absolute error for the ^{13}C (●), ^{15}N-Nitro (○) and ^{15}N-Amine (▲) NMR calculations at different models using different basis set. The geometry optimizations of the structures utilized as inputs were performed at B3LYP/6-311+G(D,P) theory level.

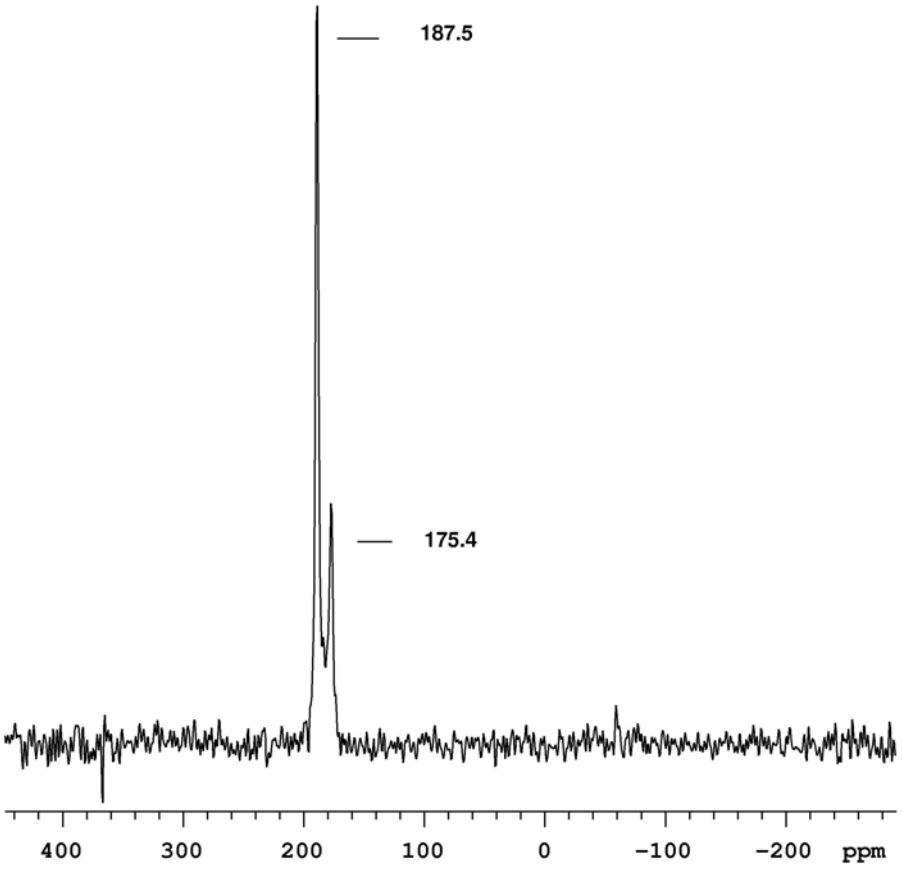

Figure 5.4 Solid-state CP/MAS ^{15}N NMR spectrum of RDX.

Two possible structures with C_{3V} symmetry are possible in solution; all nitro groups occupying axial positions (AAA conformer) and all nitro groups occupying pseudo-equatorial positions. Theoretical predictions of chemical shifts indicate that the molecular geometry of RDX, in solution, is consistent with the AAA conformer. On the other hand, the solid-state CP/MAS ^{13}C NMR spectrum of RDX exhibited a single peak at 61.5 ppm, close to liquid state chemical shift of 60.8 ppm in deuterated dimethylsulfoxide. The ^{13}C NMR chemical shift is less susceptible to the chemical environment for the polymorphs of RDX.

One of the most valuable properties of the chemical shieldings is their sensitivity to the molecular geometry and environment. The experiments provided only the values of chemical shifts, which were later assigned in to the molecular frame by comparison with the calculated values. The high accuracy achievable by modern chemical shieldings calculations allows its use in revising questionable assignments.

6 CONCLUSIONS

Isotopic Studies of α-RDX

Infrared and Raman spectra of the cyclic nitramine α-RDX, and ^{13}C, and ^{15}N (on ring) enriched RDX analogues in the solid state were recorded and their fundamental frequencies have been assigned using isotopic frequency shifts. The IR and Raman spectra for α-RDX and its isotopic derivatives were also computed using density functional calculations and compared with the normal isotopic experimental spectra. The results of the calculations were in reasonable agreement with the observed wavenumber locations, in most of the cases. DFT have also allowed more definitive set of assignments to be made for α-RDX and its isotopomers. The experimental results obtained in this study for RDX, $^{13}C_3$RDX and $^{15}N_3$RDX compared with theoretical data allowed to derive correlations of observed frequency deviations of certain vibration modes and the effect of isotopic substitution on the RDX molecule. Most of the observed vibrational bands have been successfully assigned by the present work.

α→β Phase Transition of RDX

The presented results show that FT-Raman spectroscopy can be used to clearly detected phase transitions in α-RDX. The solid-solid phase transition behavior between the polymorph forms was studied at temperature induced and the FT-Raman spectra recorded at isothermal conditions.

A systematic study of the changes in the Raman spectra of RDX to 204°C has been presented. The Raman vibrational patterns observed below 204°C are consistent with those previously defined for α-RDX. The α→β transition is supported by the vibrational modifications, such as the decreasing of number of the vibrational modes and intensity changes. The decrease in the number of peaks in the Raman spectra is in general indicative of the increasing of molecular symmetry.

Using Raman spectroscopy we have observed the solid-solid phase transition of RDX in real time. By heating at slow rates and following the spectral details, crystal transformation occurring near the melting point can be seen. The results from these experiments show that once formed the β-RDX no reversible change in the symmetry is observed and the Raman spectra differences in both conformers are evident.

^{13}C and ^{15}N Chemical Shifts Calculations on Nitramines

In order to suggest a convenient and consistent protocol to be employed for mimicking the experimental ^{13}C and ^{15}N spectra of nitramine compounds, different combinations of models and basis sets were considered. The CSGT is a better model than GIAO to evaluate the gauge origin of the vector potential describing the external magnetic field for the compounds studied here. The B3LYP/6-311+G(2d,p) level and CSGT model can be used to calculate ^{13}C and

^{15}N NMR chemical shifts with a very high accuracy and a dramatic reduction of the computational time for nitramine compounds.

The most reliable results were obtained at B3LYP/6-311+G(2d,p) level and CSGT model and can be used to calculate ^{13}C and ^{15}N NMR chemical shifts with a very high accuracy and a dramatic reduction of the computational time for nitramine compounds. The theoretical results of chemical shielding obtained in this study for RDX compared with experimental results indicates ^{15}N-amine NMR chemical shift sensitivity to the molecular geometry. These results shows that the agreement between theoretical and experimental ^{15}N-amine NMR chemical shieldings of nitramines could be used for evaluate the intrinsic relationship between structure and explosives properties.

REFERENCES

Bachman, W. E. and Sheena, J. C., 1949. A new method of preparing the high explosive RDX. J. Am. Chem. Soc., 71:1842-1845.

Baer, B. J. Oxley, J. and Nicol, M., 1990. The phase diagram of RDX (Hexahydro- 1,3,5-trinitro-s-triazine) under hydrostatic pressure", High Pressure Research 2: 99-108.

Becke, A. D., 1988. Density-functional exchange-energy approximation with correct asymptotic behavior. Phys. Rev A., 38: 3098-3100.

Becke, A. D., 1993. A new mixing of Hartree-Fock and local density-functional theories. J. Chem. Phys., 98: 1372-1377.

Bouman, T. D. and Hansen A. E., 1989. Linear response calculations of molecular optical and magnetic properties using RPAC program. Int. J. Quantum Chem. Symp. 23: 381-386.

Brill, T., Sergio, T. and Karpowicz R.,1983. β-Polymorph of hexahydro-1,3,5-trinitro-s-triazine. A Fourier Transform infrared spectroscopy study of an energetic material. Ind. Eng. Chem. Prod. Res. Dev., 22: 363-365.

Bulusu, S., Axenrod, T. and Autera J. R., 1981. Application of ^{13}C and ^{15}N NMR spectroscopy to structural studies on nitramines. Organic Magnetic Resonance.16: 52-56.

Castro, M., P., Cotte, I., Hernández S. P., Mina, N., Santana A., Chamberlain, R. T. and Lareau R., 2004. Vibrational spectroscopy study of β and a RDX deposits. J. Phys. Chem. B., 108: 8799-8805.

Castro-Rosario, M., Mercado, L., Torres, P., Gómez, L. M., Mina, N., Hernández, S. P., Lareau, R. and Chamberlain, R. T., 2004 “Synthesis and Characterization of High-Energy Nanoparticles”, J. Phys. Chem. B, 108: 12314-12317.

Cheeseman, J. R., Trucks G. W., Keith T. A. and Frisch J. M., 1996. A comparison of models for nuclear magnetic resonance shielding tensors. J. Chem. Phys., 104: 5497-5508.

Choi, C. and Prince, E., 1972. The crystal structure of cyclotrimethylenetrinitramine. Acta Crystallogr. Sect B, 28: 2857-2860.

Ciezak, J. A., Jenkins, T. A., Liu, Z., and Hemley, R. J., 2007. High-pressure vibrational spectroscopy of energetic materials: Hexahydro-1,3,5-trinitro-triazine. J. Phys. Chem. A, 111: 59-63.

Cramer, C. J. 2004. Essentials of Computational Chemistry: theories and models, Wiley and Sons, Inc., New York, NY, pp. 607.

Ditchfield, R., 1974. Self consistent perturbation theory of diamagnetism. A gauge-invariant LCAO method for NMR chemical shifts. Mol. Phys., 27: 789-794.

Dreger, A. Z. Patterson, J. E. and Gupta, Y. M., 2007. Shock wave-induced phase transition in RDX single crystals. J. Phys. Chem. B, 111: 10897-10904.

Dunning T. H. and Woon D., 1995. Gaussian basis sets for use in correlated molecular calculations. I. The atoms boron through neon and hydrogen J. Chem. Phys. 90: 1007-1017.

Facceli, J. A., 2004. Calculations of chemical shieldings: theory and applications. Concepts in Magnetic Resonance Part A. 20: 42-69.

Filhol, A., Clement, C., Forel, M. T., Pavot, J., Rey-Lafon, M., Richoux, G., Trinquecoste, C. and Cherville, J., 1971. “Molecular Conformation of 1,3,5-Trinitrohexahydro-s-triazine (RDX) in solution”. J. Phys. Chem. 75(13): 2056-2060.

Foreman, J. B. and Frisch, A., 1996. Exploring chemistry with electronic structure methods. Gaussian, Inc., Pittsburgh, 302 pp.

Freitag, M. A., Hillman B. and Agrawal, A., 2004. Predicting shielding constants in solution using gauge invariant atomic orbital theory and effective fragment potential method. J. Chem Phys. 120(3): 1197-1202.

Frish, A., Dennington, R. D., Keith, T.A, Nielsen, A. B. and Holder, A. J., 2003. Gaussview 03.

Frisch, M. J., Trucks, G. W., Schlegel, H. B., Scuseria, G. E., Robb, M. A., Cheeseman, J. R., Zakrzewski, V. G., Montgomery, Jr. J. A., Stratmann, R. E., Burant, J. C., Dapprich, S., Millam, J. M., Daniels, A. D., Kudin, K. N., Strain, M. C., Farkas, O., Tomasi, J., Barone, V., Cossi, M., Cammi, R., Mennucci, B., Pomelli, C., Adamo, C., Clifford, S., Ochterski, J., Petersson, G. A., Ayala, P.Y., Cui, Q., Morokuma, K., Malick, D. K., Rabuck, A. D., Raghavachari, K., Foresman, J. B., Cioslowski, J., Ortiz, J. V., Baboul, A.

G., Stefanov, B. B., Liu, G., Liashenko, A., Piskorz, P., Komaromi, I., Gomperts, R., Martin, R. L., Fox, D. J., Keith, T., Al-Laham, M. A., Peng, C. Y., Nanayakkara, A., Gonzalez, C., Challacombe, M., Gill, P. M. W., Johnson, B. G., Chen, W., Wong, M. W., Andres, J. L., Head-Gordon, M., Replogle, E. S. and Pople, J. A., 2003. GAUSSIAN 03 (Revision A.9), Gaussian, Inc., Pittsburgh.

Gabor, M. and Pulay, P., 2003. Assessment of density functional methods for nuclear magnetic resonance shielding calculations. J. Chem. Phys., 119: 1350-1357.

Gauss, J. and Stanton, J. F., 2002. Electron-correlated approach for calculation of NMR chemical shifts. Adv. Chem. Phys., 123: 355-422.

Goto, N., Fujihsia, H., Yamawaki, H., Wakabayashi K., Nakayama Y., Yoshida M and Koshi, M., 2006. Crystal structure of the high-pressure of hexahydro-1,3,5-trinitro-1,3,5-tiazine (γ-RDX). J. Phys. Chem. B., 110: 23655-23659.

Harris, N. J. and Lammertsma K., 1997. Ab Initio density functional computations of Conformations and Bond Dissociation Energies for Hexahydro-1,3,5-trinitro-1,3,5-triazine. J. Am. Chem. Soc., 119(28): 6583-6589.

Henre, W. H., Radom, L., Schleger, P. R. and Pople, J. A., 1986. Ab initio molecular orbital theory, Wiley and Sons, Inc. New York, NY, 548 pp.

Hiroshi, Y. and Akito, E., 2000. Density functional vibrational analysis using wavenumber-linear scale factors. Chem. Phys. Lett., 325: 477-483.

Hohenberg, P. and Kohn, W. 1964. Inhomogeneus electron gas. Physical review, 136: 864-872.

Huang F., Schulkin, B., Altan, H., Federici, J., Gary, D., Barat R. Zimdars, D., Chen, H. and Tanner D. Terahertz study of 1,3,5-trinitro-s-triazine by time-domain and Fourier transform infrared spectroscopy. Appl. Phys. Lett., 85: 5535-5537.

Infante-Castillo R. and Hernandez-Rivera, S. P., 2006. Theoretical and experimental vibrational and NMR studies of RDX. Sensors, and Command, Control, Communications, and Intelligence (C3I) Technologies for Homeland Security and Homeland Defense V; Edward M. Carapezza, Ed. Proc. of SPIE. Vol. 61 62012F, 1-6.

Infante-Castillo R. and Hernandez-Rivera, S. P. 2007. Effects of isotopic substitution on the vibrational spectra of RDX. Sensors, and Command, Control, Communications, and Intelligence (C3I) Technologies for

Homeland Security and Homeland Defense V; Edward M. Carapezza, Ed. Proc. of SPIE. Vol. 6538 653825, 1-7.

Infante-Castillo, R., Rivera-Montalvo, L. A. and Hernandez-Rivera S. P., 2008. Theoretical DFT, Vibrational and NMR studies of benzimidazole and alkyl derivatives. J. Mol. Struct., 10: 887-898.

Karpowicz, R. J. and Brill, T. B., 1984. Comparison of the molecular structure of hexahydro-1,3,5-trinitro-s-triazine in the vapor, Solution, and solid phases. J. Phys. Chem., 88(3): 348-352.

Karpowicz, R. J. and Brill, T. B., 1983. "Vibrational Motion of Hexahydro-1,3,5-trinitro-s-triazine Based on the Temperature Dependence of the Nitrogen-14 Nuclear Quadrupole Resonance Spectra: The Relationship to Condensed-Phase Thermal Decomposition". J. Phys. Chem., 87(12): 2109-2112.

Keith, T. A. and Bader R., 1992. Calculation of magnetic response properties using atoms in molecules. Chem. Phys. Lett., 210: 223-231.

Keith, T. A. And Bader R., 1993. Calculation of magnetic response properties using a continuous set of gauge transformations. Chem. Phys. Lett., 179: 479-482.

Kim, K. and Jordan, K. D., 1994. Comparison of density functional and MP2 calculations on the water monomer and dimer. J. Phys. Chem. 105: 10089-10094.

Kohn W. and Sham L. J., 1965. Self-consistent equations including exchange and correlation effects. Physical Review. 140A: 1133-1138.

Kohn, W. Becke, A. D. and Parr, R. G., 1996. Density functional theory of electronic structure. J. Phys. Chem., 100: 12974-12980.

Lee, C., Yang, W. and Parr, R. G., 1988. Development of the Colle-Salvetti correlation-energy formula into a functional of the electron density. Phys. Rev. B. 37: 785-790.

Miller, P. J., Block, S. and Piermarini, G., 1991. Effects of pressure on the thermal decomposition kinetics, chemical reactivity and phase behavior of RDX Combustion and Flame, 83: 174-184.

Oxley, J., Smith J., Zheng, W., Rogers, E. and Coburn, M., 1997. Thermal decomposition of 1,3,3-trinitroazetidine (TNAZ). J. Phys. Chem. A. 101: 4375-4283.

Pople, J. S., Frisch, M.J., and Binkley, I., 1984. Self-consistent molecular orbital methods. J. Chem. Phys. 80: 3265-3269.

Rice, B. M. and Vladimiroff, T., 2002. Reinvestigation of the gas-phase structures using density functional theory predictions of electron-scattering intensities. J. Phys. Chem., 106A (43): 10437-10443.

Rice, B. M. and Chabalowski, P. D., 1997. Ab initio and nonlocal density functional study of 1,3,5-trinitro-s-triazine (RDX) conformers. J. Phys. Chem. 1997, 101A(46): 8720-8726.

Roothan, C. C. J., 1951. New developments in molecular orbital theory. Rev. Mod. Phys, 23: 69-81.

Schindler, M. and Kutzelning, W., 1982. Theory of magnetic susceptibilities and NMR chemical shifts in terms of localized quantities. J. Chem Phys., 76: 1919-1925.

Stephens, P. J., Devlin, F. J., Chabalowski, C. F. and Frisch, M. J., 1994. Ab initio calculation of vibrational absorption and circular dichroism spectra using density functional force fields. J. Phys. Chem., 98: 11623-11627.

Tormena, C. F. and da Silva G. V. J., 2004. Chemical shifts calculations on aromatic systems: a comparison of model and basis sets. Chem. Phys Lett. 398: 466-470.

Trinquecoste, C., Rey-Lafon, M. and Forel, M. T., 1975. “Détermination du Champ de Force de Valence des Modes Normaux et des Amplitudes Quadratiques Moyennes de Vibration de la Trinitro-1,3,5 Hexahydro-s-Triazine”. Journal de Chime Physique. 72(6): 689-696.

Vosko, S., Wilk, L. and Nusair, M., 1980. Accurate spin-dependent electron liquid correlation energies for local spin density calculations: a critical analysis. Canadian J. Phys, 1200-1208.

Yoo, C. S., Cynn, H., Howard, W. and Holmes, M., 1999. Equation of state, phase transition, decomposition of β-HMX (octahydro-1,3,5,7-tetranitro-1,3,5,7-tetrazocine) at high pressures. J. Chem. Phys. 111: 10229-10235.

Zeman, S. 1999. Analysis and predictions of the Arrhenius parameters of low temperature thermolysis of nitramines by means of the ^{15}N NMR spectroscopy. Thermochimica Acta., 333: 121-129.

Zeman, S., 2006. New aspects of initiation reactivities of energetic materials

demonstrated on nitramine. J. of Hazardous Materials, A132: 155-164.